The Astrophysical Journal, 904:80 (15pp), 2020 November 20 https://doi.org/10.3847/1538-4357/abbd3b

Discriminating between Neutron Stars and Black Holes with Imperfect Knowledge of the Maximum Neutron Star Mass

Reed Essick[1] and Philippe Landry[2]
[1] Kavli Institute for Cosmological Physics, The University of Chicago, Chicago, IL 60637, USA; reed.essick@gmail.com
[2] Gravitational-Wave Physics & Astronomy Center, California State University, Fullerton, 800 N State College Blvd., Fullerton, CA 92831, USA; plandry@fullerton.edu
Received 2020 July 8; revised 2020 September 9; accepted 2020 September 28; published 2020 November 23

Abstract

Although gravitational-wave signals from exceptional low-mass compact binary coalescences, like GW170817, may carry matter signatures that differentiate the source from a binary black hole system, only one out of every eight events detected by the current Advanced LIGO and Virgo observatories are likely to have signal-to-noise ratios large enough to measure matter effects, even if they are present. Nonetheless, the systems' component masses will generally be constrained precisely. Constructing an explicit mixture model for the total rate density of merging compact objects, we develop a hierarchical Bayesian analysis to classify gravitational-wave sources according to the posterior odds that their component masses are drawn from different subpopulations. Accounting for current uncertainty in the maximum neutron star mass and adopting a power-law mass distribution with or without a mass gap and either random or mass-ratio-dependent pairing, we examine two recent events from the LIGO–Virgo Collaboration's third observing run, GW190425 and GW190814. For population models with no overlap between the neutron star and black hole mass distributions, we typically find that there is a $\gtrsim$70% chance, depending on the exact population model, that GW190425 was a binary neutron star merger rather than a neutron-star–black-hole merger. On the other hand, we find that there is a $\lesssim$6% chance that GW190814 involved a slowly spinning neutron star, regardless of our assumed population model.

Unified Astronomy Thesaurus concepts: Gravitational waves (678); Neutron stars (1108); Black holes (162); Compact objects (288);

1. Introduction

Most of the compact binary coalescences observed during the first two observing runs of the Advanced LIGO (Aasi et al. 2015) and Virgo (Acernese et al. 2015) detectors (O1 and O2) were neatly categorized as binary black hole (BBH) systems based on their inferred masses, which comfortably exceed the maximum neutron star (NS) mass of 3–4 $M_\odot$ derived from basic causality arguments (Rhoades & Ruffini 1974; Van Oeveren & Friedman 2017). However, during the detectors' third observing run (O3), the LIGO–Virgo Collaboration (LVC) reported a number of low-mass systems that cannot be categorized so easily. GW190425, a compact binary coalescence with a total mass of approximately 3.4 $M_\odot$, was deemed a likely binary NS (BNS) merger because its component masses lie between 1.12 and 2.52 $M_\odot$ (Abbott et al. 2020), compatible with many models of NS structure. Although it is very likely that this system was a BNS, because no unequivocal matter effects were discernible in the gravitational-wave (GW) signal and no electromagnetic (EM) counterpart was identified, there is no definitive proof that the system contained an NS (Han et al. 2020; Kyutoku et al. 2020). Similarly, GW190814 (Abbott et al. 2020b) has a secondary mass of 2.5–2.7 $M_\odot$, potentially consistent with either an NS or a black hole (BH). Even the nature of GW170817 (Abbott et al. 2017a), the seminal discovery from O2, is somewhat ambiguous (Abbott et al. 2017b, 2017c, 2019, 2020a; Coughlin & Dietrich 2019; Hinderer et al. 2019; Essick et al. 2020).

Accurately classifying compact binary coalescences is important for studies of NS matter, the interpretation of electromagnetic counterparts, and inferences of subpopulation properties. For example, mistaking BHs for NSs can bias our knowledge of the NS equation of state (Yang et al. 2018; Chen & Chatziioannou 2020). Kilonova models, including those used to estimate the amount of dynamical ejecta associated with GW170817 (Abbott et al. 2017c), depend partly on whether the system is a BNS or an NSBH binary (e.g., Fernández et al. 2017; Barbieri et al. 2019). Likewise, certainty that GW190425 was a BNS would alter the known properties of the distribution of NS masses in binaries because it is a strong outlier compared to known Galactic BNSs (Abbott et al. 2020; Gupta et al. 2020).

Many authors have examined how well one can distinguish NSBH coalescences from BNS or BBH mergers based on their GW signals in second- (Hannam et al. 2013; Littenberg et al. 2015; Mandel et al. 2015; Johnson-McDaniel et al. 2018; Yang et al. 2018; Chen & Chatziioannou 2020; Datta et al. 2020; Tsokaros et al. 2020) and third-generation detector networks (Krishnendu et al. 2019; Chen et al. 2020; Fasano et al. 2020). These studies rely on various matter signatures in the waveform to discern the presence of an NS in the binary. Chief among these are tidal effects that imprint on the waveform during the inspiral. This manifests as a phase offset relative to an equivalent BBH system caused by the integrated effects of stationary (e.g., Flanagan & Hinderer 2008; Read et al. 2009), dynamical (e.g., Lai 1994; Reisenegger & Goldreich 1994; Hinderer et al. 2016; Steinhoff et al. 2016), and nonlinear tides (e.g., Essick et al. 2016; Weinberg 2016; Abbott et al. 2019a). The dominant part of the phase shift is due to the quasi-static equilibrium tide, parameterized by

the binary tidal deformability,

$$\tilde{\Lambda} = \frac{16}{13}\frac{(m_1 + 12m_2)m_1^4\Lambda_1 + (m_2 + 12m_1)m_2^4\Lambda_2}{(m_1 + m_2)^5}, \quad (1)$$

for component masses $m_1 \geqslant m_2$ (by convention) with tidal deformabilities Λ_1 and Λ_2, respectively. It is this combination of individual tidal parameters to which GW detectors are most sensitive. However, for very asymmetric NSBHs ($\Lambda_1 = 0$, $m_2 \ll m_1$) or massive BNSs ($\Lambda_1, \Lambda_2 \to 0$), $\tilde{\Lambda}$ can become very small, so as to be pragmatically indistinguishable from a BBH ($\tilde{\Lambda} = 0$). This poses a not-insignificant limitation on the use of tides to distinguish NSs from BHs (Johnson-McDaniel et al. 2018; Yang et al. 2018; Chen & Chatziioannou 2020; Chen et al. 2020; Fasano et al. 2020; Tsokaros et al. 2020), as the systems about which we are most uncertain are precisely those for which tidal deformations are difficult to resolve.

Several as-yet unmeasured waveform signatures could also potentially discriminate between NSs and BHs in merging compact binaries. An abrupt truncation of the GW waveform, the unmistakable sign of tidal disruption (Shibata & Taniguchi 2008), would be a clear hallmark of an NSBH. The lack of an EM counterpart may also distinguish between a BBH and similar NSBH or BNS systems (Foucart et al. 2018; Coughlin et al. 2019; Barbieri et al. 2020). However, this requires a robust prediction for the amount of luminous matter left outside the merger remnant, and if the primary mass is sufficiently large or the BH spin is sufficiently small, the lighter companion could be swallowed whole. Modifications of the GW inspiral due to a spin-induced quadrupole moment (Krishnendu et al. 2017, 2019) or tidal heating (Datta et al. 2020) can also distinguish BHs from NSs, at least in principle, but it is unclear whether these effects will be measurable with second- or third-generation detectors. Future detector networks might also be able to distinguish the nature of the premerger components through direct observations of the postmerger remnant (Tsokaros et al. 2020).

The issues with classification schemes based on GW matter signatures are compounded by the fact that most detections made with the current advanced detectors will be near the detection threshold, and therefore matter signatures may be difficult to resolve (Lackey & Wade 2015). Indeed, 87.5% of events detected above a threshold signal-to-noise ratio (S/N) of 10 are expected to have $\mathrm{S/N} < 20$, the threshold beyond which tidal effects are generally measured well. The case may be more optimistic for third-generation detectors (e.g., Vitale 2016; Haster et al. 2020), but there will always be a population of poorly resolved events at the sensitivity threshold. EM counterparts may help distinguish between types of binaries (Hannam et al. 2013; Yang et al. 2018; Hinderer et al. 2019; Margalit & Metzger 2019), but these may not always be detectable, particularly for broadly localized, distant sources (Coughlin et al. 2019).

In any case, we can reliably expect the component masses to be better constrained by GW data than the tidal deformabilities because they enter in the waveform at lower post-Newtonian orders (Flanagan & Hinderer 2008; Read et al. 2009). Fortunately, even without any tidal information, the component masses are still informative. Several authors have already investigated mass-based classification schemes. Following the initial work by Hannam et al. (2013), Littenberg et al. (2015) quantified the typical uncertainty in mass measurements and whether posterior credible intervals will likely be small enough to confidently distinguish between NSs and BHs. Specifically, they found that objects with true masses $\lesssim 1.4\,M_\odot$ should be confidently identified as NSs (i.e., below an assumed mass gap of 3–5 $M_\odot$) while objects with masses $\gtrsim 6\,M_\odot$ should be confidently identified as BHs. Mandel et al. (2015) explored the ability to distinguish between NSs and BHs with masses based on credible intervals assuming a single expected mass distribution from population synthesis calculations. Additionally, Mandel et al. (2016) explored model-independent clustering schemes to identify different types of compact object mergers based on their masses, validating their approach by recovering population synthesis predictions with simulated measurement uncertainty. Each of these studies only considered mass distributions with large mass gaps between NSs and BHs, and they used posterior credible intervals instead of full posterior distributions.

Kapadia et al. (2020) implemented a multiclass classification scheme based on component masses and spins inferred from a template-based GW search. This was used to compute probabilities that individual GW events were astrophysical in origin for the LVC's GWTC-1 catalog (Abbott et al. 2019b). However, they assumed component mass distributions that were not informed by the observed set of detections and chose fixed boundaries between classes a priori. Classification updates released by the LVC during O3 (The LIGO Scientific Collaboration & The Virgo Collaboration 2020a, 2020b), based on parameter estimation from GW data, used the full mass posteriors, although they still employed fixed boundaries between classes.

In this paper, we implement a mass-based classification for GW sources. While the uncertainty in the compact objects' masses plays a decisive role in our approach, we directly derive posterior odds based on the full component mass posteriors. We generalize Kapadia et al. (2020) and The LIGO Scientific Collaboration & The Virgo Collaboration (2020a) by giving a complete treatment of the mass distributions, accounting in particular for uncertainty in the maximum NS mass.

We present a hierarchical Bayesian model selection scheme to determine whether individual compact objects are NSs or BHs based on their masses. We show how to self-consistently infer the mass distribution while updating our knowledge of individual events. For concreteness, we apply our method to two recent GW events of ambiguous nature, GW190425 and GW190814. We restrict our population models to a few limiting cases in order to show the classification's sensitivity to the assumed mass distribution. Our examples are not meant as a comprehensive census of proposed low-mass distributions, but rather capture the effects of a few common phenomenological features. Additionally, we describe the types of uncertainty that limit the inference. While Bayesian classification schemes of this kind are applicable to other problems in astrophysics, such as X-ray binaries (e.g., Gopalan et al. 2015), here we provide a treatment tailored specifically for GW sources.

Of tantamount importance to our analysis is the uncertainty in $M_{\rm max}$, the maximum gravitational mass an NS can attain. For nonrotating stars, the maximum mass ($M_{\rm TOV}$) is set by the equation of state (EOS) of NS matter, which determines the internal pressure gradients that oppose gravitational collapse. As we do not know the EOS perfectly, there remains considerable uncertainty in $M_{\rm TOV}$. In general, rotation can support more massive stars against collapse so that $M_{\rm max}$ is a

function of both $M_{\rm TOV}$ and the object's dimensionless spin $\chi = cS/Gm^2$, where S is the object's spin angular momentum, with $\lim_{\chi\to 0} M_{\rm max} = M_{\rm TOV}$ (e.g., Breu & Rezzolla 2016). Specifically, we approximate the effects of solid-body rotation; differential rotation can temporarily support stars of even higher masses but is not stable for viscous fluids.

Additionally, astrophysical formation channels, including any accretion or spin-up after the NS is born in a core-collapse supernova, may only produce NSs up to a mass scale $M_{\rm form} \leqslant M_{\rm max}$. Although we can still take $M_{\rm max}$ as a reasonable upper bound without asserting detailed knowledge of such formation channels, we are still sensitive to the (somewhat unknown) shape of the population of merging compact objects, along with our uncertainty in $M_{\rm max}$.

We briefly summarize our main conclusions in Section 1.1 before presenting our hierarchical Bayesian methodology in Section 2. Section 3 describes how we incorporate (uncertain) knowledge of the distribution of low-mass stellar remnants and the NS maximum mass in our inference. Section 4 applies our methodology to classify GW190425 and GW190814 in greater detail. In Section 5, we explore how a definite source classification for an event can improve our knowledge of its properties and those of the compact object population. Finally, we conclude in Section 6.

1.1. Executive Summary

Before laying out our formalism in detail, we briefly summarize the results of our case studies. We classify the binary coalescences GW190425 and GW190814 as BNSs, NSBHs, or BBHs on the basis of their component masses, assuming that the NS and BH mass distributions do not overlap while accounting for uncertainty in both $M_{\rm max}$ and the overall astrophysical distribution of component masses. We take each component mass's overall prior distribution to be either uniform, a power law, or a power law with a mass gap, and assume either a random or mass-ratio-dependent pairing function. Additionally, we consider $M_{\rm max}$ distributions inferred from EOS and population studies of NSs. This is illustrated in Figure 1, which shows how the m–$M_{\rm TOV}$ parameter space is partitioned into NS-compatible and NS-incompatible regions.

The existence of $\sim 2\ M_\odot$ NSs implies that GW190425's secondary component of 1.12–1.68 $M_\odot$ is an NS, while its primary component of 1.61–2.52 $M_\odot$ could be either an NS or a BH, depending on $M_{\rm max}$. We quantify this by calculating $P(m_1 \leqslant M_{\rm max})$ for different uncertain estimates for $M_{\rm max}$ and choices of the unknown compact object mass distribution. The different scenarios and their resulting probabilities are given in Table 2. We find the probability that GW190425's primary is an NS to be generally $\gtrsim$70%, no less than 60%, and often $\gtrsim$90%. Hence, GW190425 is likely a BNS on the basis of its component masses.

Similarly, GW190814's $\sim 23\ M_\odot$ primary component is definitely a BH, while the nature of its 2.50–2.67 $M_\odot$ secondary component is ambiguous. Calculating $P(m_2 \leqslant M_{\rm max})$ for the same scenarios as above, we arrive at Table 3. The results are essentially insensitive to the assumed population model. For the $M_{\rm TOV}$ estimates from EOS studies, there is a $\lesssim$6% chance that the secondary is a slowly spinning NS, while for the population-based $M_{\rm max}$ estimate, the probability rises to $\sim$30%. Only if we assume the secondary is spinning at the breakup frequency for an NS, and that the maximum achievable NS mass is consequently boosted by rotational support, does the probability favor an NS. Thus, we conclude that GW190814 is more likely to be a BBH than an NSBH.

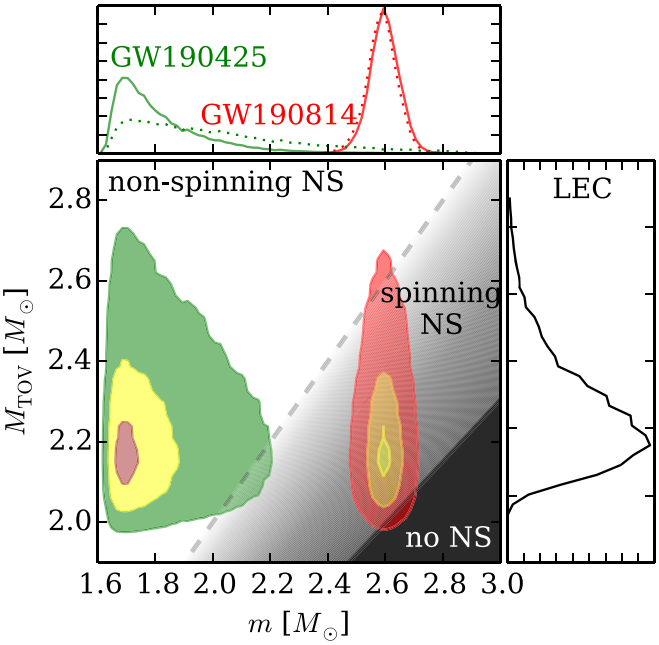

Figure 1. Joint posterior distributions for component masses and $M_{\rm TOV}$. GW190425's m_1 is shown in green and GW190814's m_2 is shown in red, assuming a power-law mass distribution with no mass gap similar to Fishbach & Holz (2020; $p_{\rm PL}(m)$ in Table 1) is relevant at low masses. The top panel compares the mass posteriors obtained with this assumed population (solid lines) against those for a uniform mass distribution (dotted lines). The $M_{\rm TOV}$ distribution, shown in the right panel, is taken from the NS EOS inference of Landry et al. (2020) (LEC). In the joint distributions, the unshaded region where $M_{\rm TOV} \geqslant m$ supports nonspinning NSs, although this region could also contain other types of stellar remnants. Therefore, the posterior probability within this region is an upper limit on the probability that the object is a nonspinning NS. Gray shading indicates the region where NSs can only exist if they are spinning, with darker shading indicating the need for larger spins. The darkest shaded region below the solid black line corresponds to regions where no stable NS can exist.

2. Distinguishing Compact Objects by Their Masses

Consider the subset of GW signals for which matter signatures, like tidal deformations, are inconclusive. We are then left with information about objects' masses as the primary way to distinguish between different types of compact binaries.

Fundamentally, we will ask whether an observed mass m is most consistent with one of several known mass distributions, all of which contribute to a mixture model representing the overall rate density of compact objects such that

$$\frac{d\mathcal{N}_{\rm tot}}{d\mu} = \sum_\alpha \frac{d\mathcal{N}_\alpha}{d\mu}. \tag{2}$$

Greek indices label the different subpopulations (e.g., m_1 is a BH and m_2 is a BH), Latin indices label the different observed systems, and μ stands for all single-event parameters, such as component masses $m_{1,2}$ and spins $\chi_{1,2}$, with the understanding that $d\mu = dm_1 dm_2 d\chi_1 d\chi_2 \cdots$.

It is common practice to parameterize the rate density as an overall rate $\mathcal{R}$ times an overall mass distribution $p(\mu|\Theta, P)$, which itself is constructed as a mixture model. That is,

$$\frac{d\mathcal{N}_{\rm tot}}{d\mu} = \mathcal{R}\, p(\mu|\Theta, P), \tag{3}$$

where

$$p(\mu|\Theta, P) = \sum_{\alpha} p(\mu|\theta_\alpha) p_\alpha, \tag{4}$$

$$p_\alpha = \frac{\int d\mu \, (d\mathcal{N}_\alpha/d\mu)}{\mathcal{R}} = \frac{\mathcal{R}_\alpha}{\sum_\beta \mathcal{R}_\beta}. \tag{5}$$

Each subpopulation is described by a mass distribution $p(\mu|\theta_\alpha)$ determined by population parameters θ_α and a prior probability p_α equivalent to its fractional contribution to the overall rate ($\mathcal{R}_\alpha/\mathcal{R}$). Θ represents the union of $\theta_\alpha \, \forall \, \alpha$, and P represents the union of all p_α. We further assume all probability distributions are normalized.

In this paper, we compare posterior probabilities that a given GW event hails from different subpopulations. We consider binaries containing only NSs and BHs, although additional populations of hypothesized exotic compact objects (see, e.g., Cardoso & Pani 2019) could easily be accommodated. Our analysis includes correlations between the masses and spins of binary components in GW mergers, as there are both theoretical (e.g., Bulik et al. 2003; Rodriguez et al. 2018, 2019) and empirical (Abbott et al. 2019c; Fishbach & Holz 2020) evidence that binaries do not form through random pairings.

2.1. Compact Object Classification

Suppose we have independent observations of N systems constituting a set $\mathcal{E}$, each with separate single-event parameters μ_i such that $\{\mu\}_\mathcal{E} = (\mu_1, \mu_2, \cdots, \mu_N)$. The nature of the kth system is unclear because of the uncertainty in both μ_k and the subpopulations. We account for both kinds of uncertainty by explicitly modeling them within our analysis. To wit, we construct a joint distribution over all the data $\{\mathcal{D}\}_\mathcal{E} = (\mathcal{D}_1, \mathcal{D}_2, ..., \mathcal{D}_N)$, single-event parameters $\{\mu\}_\mathcal{E}$, and population parameters $(\Theta, P, \mathcal{R})$ (e.g., Loredo & Wasserman 1995; Loredo 2004; Farr et al. 2015; Abbott et al. 2019c; Mandel et al. 2019):

$$p(\{\mu\}_\mathcal{E}, \mathcal{R}, \Theta, P, \{\mathcal{D}\}_\mathcal{E}) = p(\mathcal{R}, \Theta, P)\mathcal{R}^N e^{-\mathcal{R}\beta(\Theta,P)} \times \prod_{i\in\mathcal{E}}^{N} p(\mathcal{D}_i|\mu_i) p(\mu_i|\Theta, P), \tag{6}$$

where

$$\beta(\Theta, P) = \int d\mu \, P(\text{det}|\mu) p(\mu|\Theta, P) \tag{7}$$

is the probability of making a detection given the population model, which accounts for selection effects (i.e., observational biases) within the survey. $P(\text{det}|\mu)$ is the probability of detecting a system with parameters μ, and $p(\mathcal{R}, \Theta, P)$ represents our prior beliefs about all population-level parameters. Conditioning Equation (6) on the observed data yields a posterior distribution, and marginalizing over the overall rate and population parameters yields population-informed posterior distributions for the observed systems' parameters $\{\mu\}_\mathcal{E}$. Specifically,

$$p(\{\mu\}_\mathcal{E}|\{\mathcal{D}\}_\mathcal{E}) = \frac{\int d\mathcal{R} d\Theta dP \, p(\{\mu\}_\mathcal{E}, \mathcal{R}, \Theta, P, \{\mathcal{D}\}_\mathcal{E})}{\int d\mathcal{R} d\Theta dP \left(\prod_{i\in\mathcal{E}} d\mu_i\right) p(\{\mu\}_\mathcal{E}, \mathcal{R}, \Theta, P, \{\mathcal{D}\}_\mathcal{E})}. \tag{8}$$

A population-informed posterior distribution $p(\mu_k|\{\mathcal{D}\}_\mathcal{E})$ for μ_k follows from a marginalization over the other $N-1$ systems.

Similarly, we can compute the joint posterior for any individual system k to come from a subpopulation α_k by extracting the part of the overall mixture model prior for μ_k associated with α_k:

$$p(\alpha_k|\{\mathcal{D}\}_\mathcal{E}) = \frac{\int d\mathcal{R} d\Theta dP \, p(\Theta, P, \mathcal{R})\mathcal{R}^N e^{-\mathcal{R}\beta(\Theta,P)} \left(\prod_{i\neq k} d\mu_i \, p(\mathcal{D}_i|\mu_i) p(\mu_i|\Theta, P)\right) d\mu_k \, p(\mathcal{D}_k|\mu_k) p(\mu_k|\theta_\alpha) p_\alpha}{\int d\mathcal{R} d\Theta dP \left(\prod_{i\in\mathcal{E}} d\mu_i\right) p(\{\mu\}_\mathcal{E}, \mathcal{R}, \Theta, P, \{\mathcal{D}\}_\mathcal{E})}. \tag{9}$$

Comparing such posterior probabilities for different subpopulations (e.g., NSBH versus BBH) is the basis of our inference. This is done most straightforwardly by computing an odds ratio

$$\mathcal{O}^{\alpha_k}_{\beta_k} = \frac{p(\alpha_k|\{\mathcal{D}\}_\mathcal{E})}{p(\beta_k|\{\mathcal{D}\}_\mathcal{E})} \tag{10}$$

between two possible classifications α and β.

We can gain a bit more intuition for the posterior probability, Equation (9), by rewriting it as

$$p(\alpha_k|\{\mathcal{D}\}_\mathcal{E}) = q_{\alpha_k|\{\mathcal{D}\}_{\mathcal{E}\backslash k}} \int d\mu_k \, p(\mathcal{D}_k|\mu_k) q(\mu_k|\{\mathcal{D}\}_{\mathcal{E}\backslash k}, \alpha_k), \tag{11}$$

where $\{\mathcal{D}\}_{\mathcal{E}\backslash k}$ is the set of observed data from the $N-1$ systems not including the kth event,

$$q(\mu_k|\{\mathcal{D}\}_{\mathcal{E}\backslash k}, \alpha_k) = \frac{\int d\mathcal{R} d\Theta dP \, p(\mathcal{R}, \Theta, P)\mathcal{R}^N e^{-\mathcal{R}\beta(\Theta,P)} \left(\prod_{i\neq k} d\mu_i \, p(\mathcal{D}_i|\mu_i) p(\mu_i|\Theta, P)) p(\mu_k|\theta_\alpha)\right) p_\alpha}{q_{\alpha_k|\{\mathcal{D}\}_{\mathcal{E}\backslash k}}} \tag{12}$$

and

$$q_{\alpha_k|\{\mathcal{D}\}_{\mathcal{E}\backslash k}} = \frac{\int d\mathcal{R}d\Theta dP\, p(\mathcal{R}, \Theta, P)\mathcal{R}^N e^{-\mathcal{R}\beta(\Theta,P)}\left(\prod_{i\neq k} d\mu_i\, p(\mathcal{D}_i|\mu_i)p(\mu_i|\Theta, P)\right)p_\alpha}{\int d\mathcal{R}d\Theta dP\, p(\mathcal{R}, \Theta, P)\mathcal{R}^N e^{-\mathcal{R}\beta(\Theta,P)}\prod_{j\neq k} d\mu_j\, p(\mathcal{D}_j|\mu_j)p(\mu_j|\Theta, P)}. \tag{13}$$

This has the natural interpretation of a properly normalized population-informed prior distribution $q(\mu_k|\{\mathcal{D}\}_{\mathcal{E}\backslash k}, \alpha_k)$ for the systems in the subpopulation α_k and a population-informed prior probability $q_{\alpha_k|\{\mathcal{D}\}_{\mathcal{E}\backslash k}}$ of belonging to the subpopulation α_k. Indeed, the population-informed mass distribution $q(\mu_k|\{\mathcal{D}\}_{\mathcal{E}\backslash k}, \alpha_k)$ is just the single-event parameter prior $p(\mu_k|\theta_{\alpha_k})$ marginalized over the uncertainty in the population parameters conditioned on data from the $N-1$ other detections and the fact that we have detected N systems in total. In this sense, the hierarchical population inference automatically determines the correct priors for the single-event analyses by marginalizing over population-level uncertainty. Thus, if we have enough events in our catalog so that the population is measured well, we can take the measured population at face value when interpreting single events.

Alternatively, from Equation (11), we can express the odds ratio as

$$\mathcal{O}^{\alpha_k}_{\beta_k} = \mathcal{B}^{\alpha_k}_{\beta_k}\left(\frac{q_{\alpha_k|\{\mathcal{D}\}_{\mathcal{E}\backslash k}}}{q_{\beta_k|\{\mathcal{D}\}_{\mathcal{E}\backslash k}}}\right), \tag{14}$$

where

$$\mathcal{B}^{\alpha_k}_{\beta_k} = \frac{\int d\mu_k\, p(\mathcal{D}_k|\mu_k)q(\mu_k|\alpha_k, \{\mathcal{D}\}_{\mathcal{E}\backslash k})}{\int d\mu_k\, p(\mathcal{D}_k|\mu_k)q(\mu_k|\beta_k, \{\mathcal{D}\}_{\mathcal{E}\backslash k})} \tag{15}$$

is a Bayes factor given population-informed mass priors and $(q_{\alpha_k|\{\mathcal{D}\}_{\mathcal{E}\backslash k}}/q_{\beta_k|\{\mathcal{D}\}_{\mathcal{E}\backslash k}})$ serves as the population-informed prior odds.

2.2. Classification Metric: Odds Ratio versus Bayes Factor

While one might naturally attempt to distinguish between possible types of compact binaries based on the Bayes factor $\mathcal{B}^\alpha_\beta$ in an attempt to minimize the impact of the prior odds in Equation (14), it turns out that $\mathcal{O}^\alpha_\beta$ is actually less sensitive to prior assumptions. Consider the following, in which we omit the label k for the compact object of interest. Assuming a fixed population so that $q(\mu|\{\mathcal{D}\}_{\mathcal{E}\backslash k}, \alpha) = p(\mu|\theta_\alpha)$ and focusing for the moment on a comparison between the NSBH and BBH subpopulations, we have

$$\mathcal{B}^{\rm NSBH}_{\rm BBH} = \frac{\int d\mu\, p(\mathcal{D}|\mu)p(\mu|\theta_{\rm NSBH})}{\int d\mu\, p(\mathcal{D}|\mu)p(\mu|\theta_{\rm BBH})}. \tag{16}$$

Because BBHs span a larger mass range than NSBHs (the secondary is limited to $m_2 \leqslant M_{\rm max}$), $p(\mu|{\rm BBH})$ brings along a relatively large Occam factor that can severely penalize the BBH model if the likelihood has support over only a small mass range. In other words, $\mathcal{B}^{\rm NSBH}_{\rm BBH}$ can be quite sensitive to the high-mass behavior of $p(\mu|\theta_{\rm BBH})$ even though the likelihood is vanishingly small at such large masses. We can see this more explicitly by including the normalization of the priors,

$$\mathcal{B}^{\rm NSBH}_{\rm BBH} = \frac{\int d\mu\, p(\mathcal{D}|\mu)d\mathcal{N}_{\rm NSBH}/d\mu}{\int d\mu\, p(\mathcal{D}|\mu)d\mathcal{N}_{\rm BBH}/d\mu}\left(\frac{\int d\mu\, d\mathcal{N}_{\rm BBH}/d\mu}{\int d\mu\, d\mathcal{N}_{\rm NSBH}/d\mu}\right). \tag{17}$$

If our population model predicts approximately equal numbers of NSBHs and BBHs within the likelihood's support, then the first ratio is of order unity. However, the second ratio can confound this, as the BBH mass distribution may extend to much higher masses, and there may simply be more BBHs than NSBHs in the universe. If this is the case, then we would infer that $\mathcal{B}^{\rm NSBH}_{\rm BBH} \gg 1$ based primarily on our knowledge of the high-secondary-mass BH distribution, which should be irrelevant when classifying compact binaries with low-mass secondaries.

We also note that, were we to assume approximately equal numbers of NSBHs and BBHs in the universe, and therefore equal prior odds, this would imply either an extremely steeply falling BBH number density with increasing mass or a steep feature in the total mass distribution at or below $M_{\rm max}$. In general, it is not possible to assign arbitrary prior odds to the different components of a mixture model while self-consistently fixing the shapes of both the subpopulations and overall mass distributions.

In contrast to $\mathcal{B}^{\rm NSBH}_{\rm BBH}$, the odds ratio becomes

$$\mathcal{O}^{\rm NSBH}_{\rm BBH} = \frac{\int d\mu\, p(\mathcal{D}|\mu)d\mathcal{N}_{\rm NSBH}/d\mu}{\int d\mu\, p(\mathcal{D}|\mu)d\mathcal{N}_{\rm BBH}/d\mu}, \tag{18}$$

which only depends on the number densities within the likelihood's support. That is to say, $\mathcal{O}^{\rm NSBH}_{\rm BBH}$ only depends on our knowledge of the mass distributions for masses similar to this event's. While this requires us to specify the number density of compact objects within particular mass ranges, rather than just a normalized distribution, this is a more physically relevant representation anyway. As such, we use $\mathcal{O}^\alpha_\beta$ rather than $\mathcal{B}^\alpha_\beta$ as our classification metric throughout the rest of this work.

3. Population Models

So far, we have described a general classification scheme that places no restrictions on the subpopulations. Indeed, Equation (9) allows for classification while simultaneously accounting for uncertainty from the population inference. However, as even the functional form of the overall mass distribution is not yet tightly constrained (Abbott et al. 2019c; Fishbach et al. 2020a), we are faced with several different sources of uncertainty. Section 3.1 discusses uncertainty in the overall mass distribution. Section 3.2 considers our uncertainty in the NS EOS, $M_{\rm TOV}$, and $M_{\rm max}$. Section 3.3 discusses the uncertainty in subpopulations, particularly whether the maximum NS produced in nature is limited by the formation channel rather than the EOS ($M_{\rm form} < M_{\rm max}$) and whether BHs and NSs exist within the same mass range.

Table 1
Single-component Mass Distributions Assumed in This Analysis, All Realizations of Equation (19) with Different Parameters

	α	Δ	$M_{\rm brk}$
$p_0(m)$	0.0	1.0	arbitrary
$p_{\rm PL}(m)$	−1.3	1.0	arbitrary
$p_{\rm BRK}(m)$	−1.3	0.1	2.3 $M_\odot$

Note. We note that when $\Delta = 1$, the distribution does not depend on the value of $M_{\rm brk}$. Specific combinations of these distributions are considered in Tables 2 and 3 to quantify the sensitivity to the unknown distribution of low-mass compact objects.

3.1. Overall Mass Distribution

Several authors have studied the astrophysical distribution of both NS and BH masses (see, e.g., Antoniadis et al. 2016; Fishbach & Holz 2017; Alsing et al. 2018; Abbott et al. 2019c; Farrow et al. 2019; Chatziioannou & Farr 2020; Farr & Chatziioannou 2020; Fishbach & Holz 2020; Fishbach et al. 2020b as well as the reviews in Mandel & Farmer 2018 and Postnov & Yungelson 2014). Specific distributions for NSs or BHs may be motivated theoretically through population synthesis calculations or empirically through observational surveys, and may have rather complex shapes. Nevertheless, our knowledge of the overall rate density of low-mass compact objects $d\mathcal{N}_{\rm tot}/d\mu$ may quickly become more precise than our knowledge of the subpopulation rate densities $d\mathcal{N}_\alpha/d\mu$ (Wysocki et al. 2020). This is because only relatively loud GW signals will carry enough tidal information to clearly signal the presence of an NS (Lackey & Wade 2015; Chen et al. 2020; Fasano et al. 2020; Landry et al. 2020), and we are likely to have many more quiet detections than loud detections. Furthermore, depending on the distributions of binaries containing NSs, most of the loud BNS and NSBH detections may involve NSs with $m \ll M_{\rm max}$, thereby providing little information about the upper reaches of the NS mass distribution.

We also note that the selection effects $\beta(\Theta, P)$ in our posteriors (Equations (6) and (8)) only depend on the total distribution $p(\mu|\Theta, P)$ and not on the individual subpopulation distributions $p(\mu|\theta_\alpha)$. Therefore, assuming precise knowledge of the overall mass distribution removes any dependence on selection effects from our inference when we marginalize over $M_{\rm max}$. As such, we consider several fixed overall mass distributions, rather than specifying distributions for, e.g., each of the BNS, NSBH, and BBH subpopulations. Specifically, we assume a few basic mass distributions for individual compact objects, all of which take the form

$$p(m) \propto \mathrm{H}(m \leqslant M_{\rm brk}) m^\alpha + \Delta \times \mathrm{H}(M_{\rm brk} < m) m^\alpha, \quad (19)$$

where $\mathrm{H}(\cdot)$ is the Heaviside function. We further assume the mass distribution to be independent of spin and other source properties. Our choices for the parameters α, Δ, and $M_{\rm brk}$ are listed in Table 1. The value of α is based on the inferred exponent from higher-mass BBH mergers during O1 and O2 (Abbott et al. 2019c). Equation (19) is also motivated by the expectation for a low-mass gap between NSs and BHs (Bailyn et al. 1998; Özel et al. 2010; Farr et al. 2011), which we model as a sharp decrease in the overall mass distribution at $M_{\rm brk}$. Our specific choices for $M_{\rm brk}$ and Δ are ad hoc; they are meant to simulate a sharp feature in $d\mathcal{N}_{\rm tot}/dm$ near the median of our current uncertainty in $M_{\rm TOV}$ and proposed upper limits from EM observations of AT 2017gfo (Shibata et al. 2019; Abbott et al. 2020a), although there is some disagreement about the exact value of that upper limit (e.g., Margalit & Metzger 2017; Rezzolla et al. 2018; Ai et al. 2020). However, $M_{\rm brk}$ may or may not be related to $M_{\rm max}$ (or even $M_{\rm form}$), as this would depend on the formation channel (e.g., Ertl et al. 2020); there could be BHs with $M_{\rm max} < m \leqslant M_{\rm brk}$. What's more, incorrectly assuming $M_{\rm brk} \approx M_{\rm max}$ could lead to biases in EOS constraints (Miller et al. 2019a; Landry et al. 2020). In this section, we fix $M_{\rm brk}$ but do not allow this choice to influence our uncertainty in $M_{\rm TOV}$ or $M_{\rm max}$.

Following Fishbach & Holz (2020) and Fishbach et al. (2020a), we construct joint distributions for m_1 and m_2 that are proportional to these single-component mass distributions and a pairing function, such that

$$p(m_1, m_2) \propto p(m_1) p(m_2) q^\beta \mathrm{H}(m_1 \geqslant m_2), \quad (20)$$

where $q = m_2/m_1$ and $\beta = 4$. We also consider random pairing, which corresponds to $\beta = 0$. We also explicitly impose our convention that $m_1 \geqslant m_2$. As different choices of α, β, Δ, and $M_{\rm brk}$ change our quantitative results, we report results with a few example distributions in Tables 2 and 3 to give a sense of the variability. We do not claim that these choices represent all possible mass distributions, but instead that they demonstrate general conclusions for GW190425's m_1 and GW190814's m_2.

3.2. Maximum Neutron Star Mass

Because the NS mass distribution truncates at (or below) $M_{\rm max}$, our uncertainty in $M_{\rm max}$ is directly tied to our ability to confidently identify individual objects as BHs rather than NSs. We therefore explore how our knowledge that a single subpopulation must truncate at a particular mass scale, which may be determined outside our population analysis and specified as a prior in Equation (9), affects our ability to distinguish between BHs and NSs. Previous studies assumed an exact, fixed boundary between those two subpopulations, but we instead use current knowledge from theoretical and empirical studies of NSs. We assume our uncertainty in $M_{\rm max}$ is uncorrelated with the mass of the compact object of interest, although this may not truly be the case if we simultaneously infer both the EOS and the mass distribution (Wysocki et al. 2020).

There are several estimates for $M_{\rm max}$ and $M_{\rm TOV}$ in the literature, derived from different astrophysical observables. For instance, our knowledge of $M_{\rm TOV}$ is informed by observations of massive pulsars (Antoniadis et al. 2013; Cromartie et al. 2020), GWs from GW170817 and GW190425, and X-ray timing observations of PSR J0030+0451 (Miller et al. 2019b; Raaijmakers et al. 2019; Riley et al. 2019) as well as the EM counterparts from GW170817 (Margalit & Metzger 2017; Rezzolla et al. 2018; Shibata et al. 2019; Abbott et al. 2020a; Dietrich et al. 2020). Similarly, studies of the mass distribution of Galactic NSs (Alsing et al. 2018; Farr & Chatziioannou 2020) constrain $M_{\rm form}$, a lower limit for $M_{\rm max}$. Moreover, the relation between $M_{\rm TOV}$ and $M_{\rm max}$ for rotating NSs has been investigated through numerical studies of rapidly spinning relativistic stars (e.g., Cook et al. 1994; Bauswein et al. 2013; Rezzolla et al. 2018).

Table 2
Estimates of $P(m_1 \leqslant M_{\rm max})$ for GW190425, the Posterior Probability that the Primary Component's Mass is Compatible with an NS, under Different Assumptions about the Compact Object Population (Columns) and the Maximum NS Mass $M_{\rm max}$ (Rows)

	$M_{\rm max}$	Population Prior $p(m_1, m_2)$				
		$p_0(m_1)p_0(m_2)$	$p_{\rm PL}(m_1)p_0(m_2)$	$p_{\rm PL}(m_1)p_{\rm PL}(m_2)q^4$	$p_{\rm BRK}(m_1)p_0(m_2)$	$p_{\rm BRK}(m_1)p_{\rm BRK}(m_2)q^4$
LEC	$M_{\rm TOV} \leqslant 2.3\,M_\odot$	61.67% ± 0.75%	68.99% ± 0.82%	91.9% ± 1.0%	86.09% ± 0.97%	95.7% ± 1.0%
LEC	$M_{\rm TOV}$	68.58% ± 0.69%	74.88% ± 0.73%	93.82% ± 0.87%	90.09% ± 0.84%	97.03% ± 0.89%
LVC	$M_{\rm TOV}$	62.0% ± 1.3%	68.8% ± 1.4%	90.9% ± 1.8%	83.6% ± 1.7%	94.2% ± 1.9%
FC	$M_{\rm max}$	72.9% ± 1.2%	77.9% ± 1.2%	93.6% ± 1.4%	88.7% ± 1.4%	96.0% ± 1.5%
LEC	$1.3M_{\rm TOV} \leqslant 2.7\,M_\odot$	96.5% ± 1.5%	97.6% ± 1.5%	99.7% ± 1.5%	99.7% ± 1.5%	99.9% ± 1.5%

Note. We report means ± standard deviations from Monte Carlo integration. The component mass priors are assumed to be either a uniform distribution $p_0(m)$, a power-law distribution $p_{\rm PL}(m)$, or a power-law distribution with a mass gap $p_{\rm BRK}(m)$ as defined by Equation (19) with the parameter choices listed in Table 1. The pairing of compact objects is assumed to be random or mass-ratio dependent, such that the population prior defined in Equation (20) takes the form $p(m_1, m_2) = p(m_1)p(m_2)$ or $p(m_1, m_2) = p(m_1)p(m_2)q^4$, respectively. The various $M_{\rm max}$ distributions account for different constraints on the maximum NS mass and different assumptions about the primary's spin. The first three rows assume negligible spin, such that $M_{\rm max} = M_{\rm TOV}$, and adopt the $M_{\rm TOV}$ posterior from Landry et al. (2020, LEC) or Abbott et al. (2018, LVC). The first row additionally accounts for an upper bound of $M_{\rm TOV} \leqslant 2.3\,M_\odot$ motivated by EM observations of AT 2017gfo (Shibata et al. 2019; Abbott et al. 2020a). The fourth row uses the NS population-based estimate of $M_{\rm max}$ from Farr & Chatziioannou (2020, FC), allowing for spin. The last row assumes rotation at the NS breakup frequency, such that $M_{\rm max} = 1.3\,M_{\rm TOV}$, while accounting for the upper bound of $M_{\rm max} \leqslant 2.7\,M_\odot$ on the maximum mass of a rotating NS from AT 2017gfo.

Table 3
Estimates of $P(m_2 \leqslant M_{\rm max})$ for GW190814, the Posterior Probability that the Secondary Component's Mass is Compatible with an NS, under Different Assumptions about the Compact Object Population (Columns) and the Maximum NS Mass $M_{\rm max}$ (Rows)

	$M_{\rm max}$	Population Prior $p(m_1, m_2)$				
		$p_0(m_1)p_0(m_2)$	$p_{\rm PL}(m_1)p_0(m_2)$	$p_{\rm PL}(m_1)p_{\rm PL}(m_2)q^4$	$p_{\rm BRK}(m_1)p_0(m_2)$	$p_{\rm BRK}(m_1)p_{\rm BRK}(m_2)q^4$
LEC	$M_{\rm TOV} \leqslant 2.3\,M_\odot$	$\leqslant$0.1%	$\leqslant$0.1%	$\leqslant$0.1%	$\leqslant$0.1%	$\leqslant$0.1%
LEC	$M_{\rm TOV}$	5.63% ± 0.15%	5.55% ± 0.15%	5.25% ± 0.15%	5.55% ± 0.15%	5.25% ± 0.15%
LVC	$M_{\rm TOV}$	3.47% ± 0.32%	3.41% ± 0.32%	3.18% ± 0.31%	3.41% ± 0.32%	3.18% ± 0.31%
FC	$M_{\rm max}$	29.12% ± 0.82%	29.02% ± 0.82%	28.58% ± 0.82%	29.02% ± 0.82%	28.58% ± 0.82%
LEC	$1.3\,M_{\rm TOV} \leqslant 2.7\,M_\odot$	86.9% ± 1.3%	86.4% ± 1.3%	83.6% ± 1.3%	86.4% ± 1.3%	83.6% ± 1.3%

Note. We report means ± standard deviations from Monte Carlo integration. The assumed population models and $M_{\rm max}$ distributions are the same as in Table 2. Because the smallest m_2 sample in the GW190814 posterior data is $\sim$2.3 $M_\odot$, we only provide approximate upper limits in the first row, where the maximum mass distribution is truncated to $M_{\rm max} \leqslant 2.3\,M_\odot$. We note that the first entry in the third row, which assumes $M_{\rm max} = M_{\rm TOV}$ from Abbott et al. (2018, LVC), recovers the result presented in Abbott et al. (2020b).

We explore a few proposed $M_{\rm max}$ distributions to characterize our inference's sensitivity to this uncertainty. Specifically, we use the inferred posterior distribution for the maximum gravitational mass of a nonrotating NS, $M_{\rm TOV}$, from Landry et al. (2020) based on a nonparametric analysis of massive pulsar, GW, and X-ray timing data. We compare this to an analysis of GW170817 assuming a spectral EOS parameterization (Carney et al. 2018) and $M_{\rm TOV} \geqslant 1.97\,M_\odot$ (Abbott et al. 2018), although the spectral parameterization may introduce model systematic errors (Tan et al. 2020), particularly in comparison to the nonparametric EOS inference of Landry et al. (2020).

We also study an empirical fit to observed galactic NSs (Farr & Chatziioannou 2020) that includes a $M_{\rm max}$ parameter. For the Landry et al. (2020) $M_{\rm TOV}$ prediction, we additionally investigate the effect of upper limits estimated from numerical simulations of ejected mass and kilonova luminosity coupled with observations of AT 2017gfo (Shibata et al. 2019; Abbott et al. 2020a), which suggest $M_{\rm TOV} \lesssim 2.3\,M_\odot$ and $M_{\rm max} \lesssim 2.7\,M_\odot$.

3.3. Overlap of Neutron Star and Black Hole Mass Distributions

Equation (9) suggests that we should directly marginalize over our uncertainty in $M_{\rm max}$. This is straightforward, but requires knowledge of the individual subpopulation's rate densities. While we can confidently state that NSs cannot exist with $m > M_{\rm max}$ (by definition), and there are reasons to believe that BHs do not exist below $M_{\rm max}$ (e.g., Fryer & Kalogera 2001; Belczynski et al. 2012), we cannot be certain that $d\mathcal{N}_{\rm BBH}/d\mu$ identically vanishes below $M_{\rm max}$. For example, primordial BHs could form in this mass range, pair, and merge within a Hubble time (Carr & Hawking 1974; Meszaros 1974). Given the fact that we will likely measure only $d\mathcal{N}_{\rm tot}/d\mu$ directly and not the rate densities of separate subpopulations, we restrict our study to mass distributions with no overlap between NSs and BHs. This amounts to asking whether individual objects are above or below $M_{\rm max}$, or equivalently maximizing the posterior probability that any individual object is an NS while fixing $d\mathcal{N}_{\rm tot}/d\mu$. That is, with the current uncertain state of our population knowledge, we can

confidently rule out NSs, but we cannot confirm their presence without more detailed knowledge of the subpopulations.

Similarly, astrophysical formation channels may limit NSs to masses $m \leqslant M_{\rm form} \leqslant M_{\rm max}$. Assuming $M_{\rm form} = M_{\rm max}$ also maximizes the probability that an object is an NS while fixing the overall mass distribution.

If we assume a known total mass distribution and that compact binaries are composed of only NSs and BHs, it implies the following. We denote the rate density of systems where the object in question is an NS as $d\mathcal{N}_{\rm NS}/d\mu$ (either a BNS or NSBH depending on the system) and the case where the object is a BH as $d\mathcal{N}_{\rm BH}/d\mu$ (similarly, either NSBH or BBH). Then,

$$\frac{d\mathcal{N}_{\rm NS}}{d\mu} \leqslant \int dM_{\rm max}\, p(M_{\rm max}) \frac{d\mathcal{N}_{\rm tot}}{d\mu} {\rm H}(m \leqslant M_{\rm max}), \tag{21}$$

$$\frac{d\mathcal{N}_{\rm BH}}{d\mu} \equiv \frac{d\mathcal{N}_{\rm tot}}{d\mu} - \frac{d\mathcal{N}_{\rm NS}}{d\mu}, \tag{22}$$

and therefore

$$\mathcal{O}^{\rm NS}_{\rm BH} \leqslant \frac{P(m \leqslant M_{\rm max})}{1 - P(m \leqslant M_{\rm max})} \tag{23}$$

where

$$P(m \leqslant M_{\rm max}) = \int dM_{\rm max}\, p(M_{\rm max}) \int dm\, p(m|\mathcal{D}) {\rm H}(m \leqslant M_{\rm max}). \tag{24}$$

Although Equation (24) explicitly calls out the single object's mass as the variable of interest, we remind the reader that $M_{\rm max}$ depends on $M_{\rm TOV}$ and the object's spin, and ${\rm H}(m \leqslant M_{\rm max})$ should be thought of as a condition in the multidimensional space spanned by an individual object's mass, spin, and $M_{\rm TOV}$.

Although the maximum spin an NS can attain depends on the EOS, several studies have found that the dimensionless spin will be limited to $\chi \lesssim 0.7$ (e.g., Cook et al. 1994; Haensel et al. 1995; Lattimer & Prakash 2001; Essick et al. 2020). At the same time, maximally spinning NSs without differential rotation are thought to reach masses between 1.2 and 1.3 $M_{\rm TOV}$ (Breu & Rezzolla 2016; Rezzolla et al. 2018), although some estimates can be larger (Bauswein et al. 2013). While universal relations exist that relate χ and $M_{\rm max}$ (e.g., Breu & Rezzolla 2016), which should mitigate the effects of our uncertainty in the EOS, these were constructed by considering only EOSs without strong phase transitions. As such, we primarily investigate limiting cases where either $M_{\rm max} = M_{\rm TOV}$ or $M_{\rm max} = 1.3 M_{\rm TOV}$, regardless of the object's spin. This bounds how much the scaling between $M_{\rm max}$ and χ could affect our analysis, although Figure 2 sketches the higher-dimensional inference for GW190814's m_2 with more precise knowledge of $M_{\rm max}(M_{\rm TOV}, \chi)$, similar to what is discussed in Most et al. (2020). We expect $dM_{\rm max}/d\chi$, $d^2M_{\rm max}/d\chi^2 > 0$ because, as the star oblates under the influence of its own spin, the centrifugal force at the surface will increase while the surface gravity simultaneously decreases. Therefore, we should expect a convex separatrix between NSs and BHs, such as the universal relation from Breu & Rezzolla (2016) shown in Figure 2. The convexity of the separatrix requires more extreme values of the spin to support NSs with masses significantly above $M_{\rm TOV}$, as compared to a spin-independent scaling like $M_{\rm max} = 1.3 M_{\rm TOV}$.

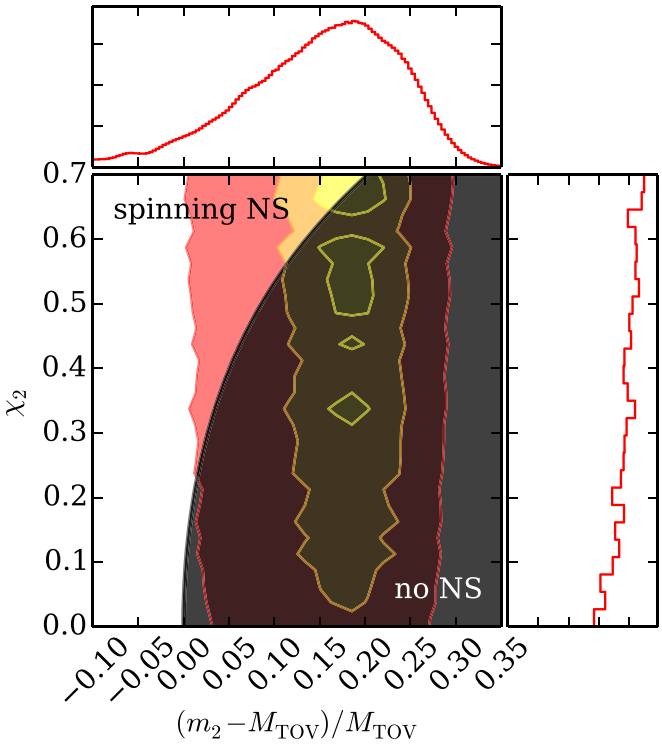

Figure 2. Joint posterior distribution for the relative difference between GW190814's m_2 and $M_{\rm TOV}$ along with the object's dimensionless spin χ_2 (shown in red). The right panel demonstrates that the spin is essentially unconstrained (the posterior is nearly identical to the prior) and uncorrelated with m_2. The main panel is divided into regions compatible (unshaded) and incompatible (shaded) with stable NSs, based on mass and spin. The separatrix is taken from the universal relation of Breu & Rezzolla (2016) between spin and the rotationally supported maximum NS mass. The bulk of the posterior probability lies within the NS exclusion zone, except if we allow for extreme values of the secondary's spin.

4. Case Studies

We calculate $P(m \leqslant M_{\rm max})$ for GW190425's primary component (Table 2) and GW190814's secondary component (Table 3) with a few choices of population models (Table 1) along with the different estimates of $M_{\rm max}$ (Section 3.2). We assume no overlap between the NS and BH mass distributions in order to maximize $P(m \leqslant M_{\rm max})$.

4.1. GW190425

GW190425 is the second BNS candidate detected by LIGO and Virgo. The secondary component of GW190425 has a mass constrained within 1.12–1.68 $M_\odot$. Given our assumption of non-overlapping NS and BH mass distributions, this immediately identifies the secondary as an NS, as we know $M_{\rm max} \gtrsim 2\, M_\odot$ (Cromartie et al. 2020). The primary component of 1.61–2.52 $M_\odot$ could, in principle, be either an NS or BH. Hence, we compute the odds ratio $\mathcal{O}^{\rm BNS}_{\rm NSBH}$ according to Equation (23), which depends only on $P(m_1 \leqslant M_{\rm max})$, to classify the primary component. We evaluate $P(m_1 \leqslant M_{\rm max})$ via Monte Carlo integrals over reweighted public posterior samples for GW190425 (The LIGO Scientific Collaboration & The Virgo Collaboration 2020c), listing the results in Table 2 given a variety of assumptions.

We find that the uncertainty in the assumed overall mass distribution leads to variation at least as large, if not larger, than

uncertainty in the $M_{\rm max}$ distribution. This is likely because GW190425 has a relatively low S/N, implying that its likelihood is not strongly peaked, and the posterior is sensitive to the assumed prior. Also, much of GW190425's m_1 posterior is below the smallest $M_{\rm max}$ allowed by any of the distributions we consider, and therefore the uncertainty in $M_{\rm max}$ does not matter for a sizable fraction of the possible m_1 values. Generally, we find that using any reasonable population prior that is not flat in both m_1 and m_2 introduces a preference for both smaller component masses and mass ratios close to unity. Both these effects tend to concentrate the m_1 posterior at lower values, thereby raising our confidence that it is below $M_{\rm max}$. Indeed, we find that it is quite likely that m_1 was a nonspinning NS, and there is only a $\lesssim$1% chance that m_1 was so large as to rule out maximally spinning NSs. While this does not prove that either of GW190425's components were NSs, it reiterates that the system is completely consistent with a BNS.

Foley et al. (2020) propose a few specific astrophysically motivated formation scenarios that, contrary to our assumptions, tend to favor more asymmetric mass ratios. They show that GW190425 is consistent with the coalescence of a low-mass BH and an NS, but do not attempt to quantify the posterior odds for that hypothesis. Similarly, Han et al. (2020) explore GW190425's consistency with an NSBH merger. Our analysis confirms that this interpretation is compatible with the data, but it suggests the event is more likely to have been a BNS merger.

4.2. GW190814

GW190814 is an unequal-mass ratio coalescence detected by LIGO and Virgo and initially announced as an NSBH candidate. An abbreviated version of this analysis in Abbott et al. (2020b) raised the strong possibility that its secondary ($m_2 \approx 2.6\,M_\odot$) was a BH rather than an NS (Abbott et al. 2020b). The nature of its $23\,M_\odot$ primary BH is not in doubt, however. We therefore compute $P(m_2 \leqslant M_{\rm max})$ to estimate $\mathcal{O}^{\rm NSBH}_{\rm BBH}$.

Table 3 reports $P(m_2 \leqslant M_{\rm max})$ for GW190814 using publicly available posterior samples (The LIGO Scientific Collaboration & The Virgo Collaboration 2020d). In this case, the effect of the population prior is negligible and instead most of our systematic uncertainty comes from the $M_{\rm max}$ distribution. This is likely because GW190814 has a higher S/N than GW190425, and its asymmetric mass ratio makes higher-order modes in the GW signal more important. The presence of detectable higher-order modes can break degeneracies within the GW waveform and improve the likelihood's constraints on q. As such, we have a much more precise constraint on m_2 that is less sensitive to our assumptions about the underlying mass distribution. This includes the presence of sharp features within $p(m|\Theta, P)$. In particular, if we include a steep mass-gap feature, it must be several orders of magnitude deep ($\Delta \lesssim 10^{-2}$) in order to select only the tail of the m_2 distribution over the much larger likelihoods at higher masses. Even if this is the case, that tail does not extend significantly below $2.3\,M_\odot$ (the smallest m_2 value from the $\sim$2800 public samples is $2.3\,M_\odot$), which is still above a significant fraction of the $M_{\rm max}$ distributions and therefore corresponds to a relatively small $P(m_2 \leqslant M_{\rm max})$. We explore the assumption of perfect mass gaps, the limit $\Delta \to 0$, in Section 5.

We also note relatively large differences when assuming $M_{\rm max}$ distributions based on constraints placed on the NS EOS from the existence of massive pulsars, GWs from coalescences known to contain at least one NS, and X-ray timing of rapidly spinning pulsars (Abbott et al. 2018; Landry et al. 2020) compared to empirical fits that are not constrained by nuclear physics (Farr & Chatziioannou 2020). This is because the empirical fit to the NS mass distribution has a much larger tail to high $M_{\rm max}$ compared to the $M_{\rm TOV}$ distributions based on the inferred EOS. We have checked that if we impose the equivalent of an upper limit of $M_{\rm TOV} \leqslant 2.3\,M_\odot$ based on EM observations of AT 2017gfo (Shibata et al. 2019; Abbott et al. 2020a) on the empirical $M_{\rm max}$ distributions, there is much better agreement between the different approaches.

Interestingly, essentially all of the m_2 posterior falls between $M_{\rm TOV}$ and $1.3\,M_{\rm TOV}$ regardless of the systematic uncertainty in $M_{\rm max}$. This means that it is unlikely that m_2 was a nonspinning NS, but m_2 remains consistent with a spinning NS. Figure 2 shows that the secondary's spin is nearly unconstrained, and therefore any finer grained inference about whether m_2 and χ_2 could correspond to an NS will depend strongly on the assumed spin prior. As such, we do not attempt to quantify this, but note that the separatrix between spinning NSs and BHs in the m–χ plane will be convex, like the universal relation reported in Breu & Rezzolla (2016). This could suggest that GW190814 is more consistent with a BBH coalescence than an NSBH, particularly if astrophysical NSs can only form with relatively small spins. Indeed, Galactic NSs in binaries that will merge within a Hubble time have $\chi \leqslant 0.05$ (Abbott et al. 2019; Essick et al. 2020), and the fastest known pulsar spin corresponds to $\chi \sim 0.35$ (Hessels et al. 2006; Essick et al. 2020), which may be small enough that $M_{\rm max} \approx M_{\rm TOV}$.

Most et al. (2020) take this line of reasoning further. Utilizing approximate universal relations for $M_{\rm max}(M_{\rm TOV}, \chi)$ from Breu & Rezzolla (2016), they bound both $M_{\rm TOV}$ and χ_2 from below, finding $M_{\rm TOV} > 2.08 \pm 0.04\,M_\odot$ and $\chi_2 \gtrsim 0.49$, as fast as or faster than the fastest known pulsar (Hessels et al. 2006). Their findings are consistent with our results, as we show that m_2 is unlikely to have been a slowly spinning NS, but they additionally assume m_2 must have been an NS at some point. They reason that the collapse from an NS to a BH must have occurred along the universal relation for $M_{\rm max}(M_{\rm TOV}, \chi)$ and correspondingly impose a tight prior on the objects spin as a function of mass. However, as we do not make these assumptions, we cannot place similar bounds.

5. Classification-informed Single-event and Population Properties

Section 4 considered the impact of our uncertainty in $M_{\rm max}$ on our ability to distinguish between NSs and BHs while assuming a fixed overall mass distribution. Here, we make a different assumption. We assume an overall mass distribution in such a way that the classification of GW190814 is definite, and then examine how that classification updates our knowledge of the EOS and $M_{\rm max}$. This shows how definite knowledge about the composition of a system can inform our knowledge of both that system's parameters and population-level parameters.

We assume that there is a perfect mass gap starting at $M_{\rm max}$ and extending to $m \sim 5\,M_\odot$. We still assume that everything below $M_{\rm max}$ is an NS, implying that BHs can only exist above $5\,M_\odot$. Similarly, we assume that the uncertainty in

$M_{\rm max}$ directly translates into uncertainty in the extent of the overall mass distribution below $\sim 5\,M_\odot$. In contrast to Section 4, this is equivalent to setting $\Delta = 0$ and $M_{\rm max} = M_{\rm brk}$ in Equation (19).

Fishbach et al. (2020b) discuss the possibility that noise fluctuations could cause detected systems to look like outliers at first glance when in fact they are entirely consistent with distributions that include sharp cutoffs. If we assume a perfect mass gap, GW190814's m_2 would be an archetypal example of such a system, as it is relatively far down the tail of our uncertainty in $M_{\rm max}$. Below, we place a simultaneous posterior over both m_2 and $M_{\rm max}$, although we ignore selection effects associated with the changes in $d\mathcal{N}_{\rm tot}/d\mu$ (now assumed to be related to $M_{\rm max}$) as the impact of GW190814's rather precise m_2 constraint is likely to be more important.

We begin with the joint posterior for $M_{\rm max}$ and GW190814's m_2,

$$\begin{aligned} p(M_{\rm max}, m_2|\mathcal{D}_{190814}, \{\mathcal{D}\}_{\varepsilon\setminus 190814}) &\propto p(M_{\rm max})p(m_2|M_{\rm max}) \\ &\times p(\{\mathcal{D}\}_{\varepsilon\setminus 190814}|M_{\rm max})p(\mathcal{D}_{190814}|m_2) \\ &= p(M_{\rm max})p(\{\mathcal{D}\}_{\varepsilon\setminus 190814}|M_{\rm max})\left(\frac{p(m_2)\mathrm{H}(m_2 \leqslant M_{\rm max})}{\int dm\, p(m)\mathrm{H}(m \leqslant M_{\rm max})}\right) \\ &\times p(\mathcal{D}_{190814}|m_2) \\ &\propto p(M_{\rm max}|\{\mathcal{D}\}_{\varepsilon\setminus 190814})\frac{\mathrm{H}(m_2 \leqslant M_{\rm max})}{\int dm\, p(m)\mathrm{H}(m \leqslant M_{\rm max})} \\ &\times p(m_2|\mathcal{D}_{190814}), \end{aligned} \tag{25}$$

where we have used the identity $p(m_2|M_{\rm max}) = p(m_2)\mathrm{H}(m_2 \leqslant M_{\rm max})/\int dm\, p(m)\mathrm{H}(m \leqslant M_{\rm max})$. If we wish to examine just the updated posterior on $M_{\rm max}$, we can marginalize over m_2 to obtain

$$\begin{aligned} p(M_{\rm max}|\{\mathcal{D}\}\,\varepsilon) &\propto p(M_{\rm max}|\{\mathcal{D}\}_{\varepsilon\setminus 190814}) \\ &\times \frac{\int dm_2\, p(m_2|\mathcal{D}_{190814})\mathrm{H}(m_2 \leqslant M_{\rm max})}{\int dm\, p(m)\mathrm{H}(m \leqslant M_{\rm max})}, \end{aligned} \tag{26}$$

which is equivalent to the expression used to incorporate data from massive pulsars in Landry et al. (2020). The prior normalization acts as an Occam factor that favors an $M_{\rm max}$ only slightly larger than the observed m_2. This term only enters if we assume a priori that m_2 is an NS. If we do not make this assumption, then the prior follows $d\mathcal{N}_{\rm tot}/dm_2$ instead of $p(m_2|M_{\rm max})$.

Similarly, we can marginalize over $M_{\rm max}$ to examine the resulting uncertainty in m_2.

$$\begin{aligned} p(m_2|\{\mathcal{D}\}\,\varepsilon) &\propto p(m_2|\mathcal{D}_{190814})p(m_2)\int dM_{\rm max} \\ &\times \frac{p(M_{\rm max}|\{\mathcal{D}\}_{\varepsilon\setminus 190814})\mathrm{H}(m_2 \leqslant M_{\rm max})}{\int dm\, p(m)\mathrm{H}(m \leqslant M_{\rm max})}. \end{aligned} \tag{27}$$

We see that the Occam factor appears again to modify the distribution of $M_{\rm max}$ from the $N-1$ other events. This effectively modifies the prior $p(m_2)$ to only include values below $M_{\rm max}$, subject to our uncertainty in $M_{\rm max}$. Recall that we have ignored selection effects in this section, meaning the fact that we have observed an Nth system is not relevant.

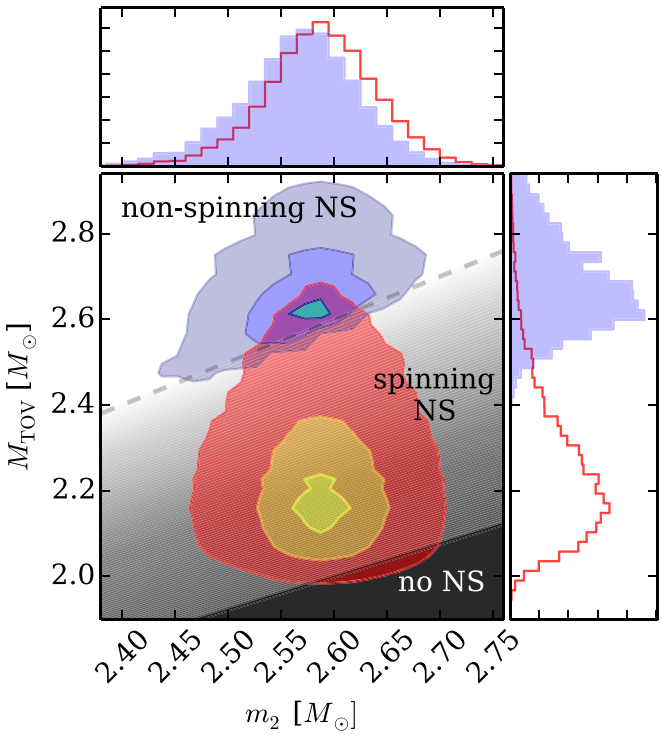

Figure 3. Distributions for GW190814's m_2 and $M_{\rm TOV}$ (LEC; Landry et al. 2020) when making no assumptions about whether m_2 is an NS or a BH (red) as well as the distributions when we assume a priori that m_2 is a nonspinning NS (blue). This analysis assumes a flat prior on m_2 that ends sharply at $M_{\rm TOV}$. We note that our knowledge of m_2 is slightly shifted to lower values, but the main effect is to shift the $M_{\rm TOV}$ posterior to larger values, although the width of the posterior remains nearly the same.

Figure 3 shows the results when we additionally assume GW190814's m_2 was slowly spinning so that $M_{\rm max} = M_{\rm TOV}$. We assume flat priors on GW190814's component masses for simplicity, as the posterior only depends weakly on the population model (see Table 3), subject to the constraint that $m_2 \leqslant M_{\rm TOV}$. Interestingly, we see that our knowledge of m_2 is not much improved, although it is shifted to slightly lower masses. Instead, the main effect of the joint inference is to retain only the tail of the $M_{\rm max}$ distribution. As this tail is nearly a power law, the size of the 90% highest-probability-density credible region only decreases by $\sim$25%, but the median is shifted above the previous 90% credible region's upper limit. Note that m_2 and $M_{\rm TOV}$ are no longer independent in the joint inference because we assume a priori that $m_2 \leqslant M_{\rm TOV}$.

Table 4 lists the original credible regions for both GW190814's m_2 and uncertainty in the NS EOS from Landry et al. (2020) as well as updated constraints obtained from this joint inference. We note that our knowledge of the pressure at even relatively low densities is somewhat affected by this inference, as it is difficult to support nonspinning NSs as large as m_2 without an exceptionally stiff EOS. Indeed, the pressure at nuclear saturation density (ρ_0) is pushed to lower values in order to match existing constraints on the radius and tidal deformability for stars with $m \sim 1.4\,M_\odot$ from GW170817 and X-ray timing observations. The value of the canonical radius is

Table 4
Medians and 90% Highest-probability-density Credible Regions for GW190814's m_2 and Observables Derived from Our Uncertainty in the NS EOS

	Original	$m_2 \leqslant M_{\rm TOV}$	Δ/CR
GW190814's m_2 [$M_\odot$]	$2.588^{+0.087}_{-0.086}$	$2.569^{+0.087}_{-0.095}$	−10%
$M_{\rm TOV}$ [$M_\odot$]	$2.22^{+0.30}_{-0.20}$	$2.67^{+0.23}_{-0.16}$	+90%
$R_{1.4}$ [km]	$12.32^{+1.09}_{-1.47}$	$12.46^{+0.96}_{-1.10}$	+5%
$\Lambda_{1.4}$	451^{+241}_{-279}	540^{+248}_{-181}	+17%
$p(\rho_0)$ [10^{33} dyn cm^{-2}]	$4.3^{+3.8}_{-4.0}$	$3.0^{+4.0}_{-2.8}$	−17%
$p(2\rho_0)$[10^{34} dyn cm^{-2}]	$3.8^{+2.7}_{-2.9}$	$5.4^{+4.5}_{-3.9}$	+29%
$p(4\rho_0)$[10^{35} dyn cm^{-2}]	$3.4^{+1.8}_{-1.2}$	$6.1^{+2.4}_{-1.9}$	+90%
$p(6\rho_0)$[10^{35} dyn cm^{-2}]	$8.6^{+5.3}_{-4.3}$	$14.3^{+6.1}_{-9.1}$	+59%

Note. We only consider a flat mass distribution for m_2 up to $M_{\rm TOV}$, as the shape of the mass distribution was found in Section 4 not to significantly affect our knowledge of m_2. We also present the change in the medians divided by the original size of the 90% highest-probability-density credible region (Δ/CR), emphasizing that the EOS observables associated with the highest densities are the most affected.

nearly unchanged, and the canonical tidal deformability changes by a smaller amount than the pressure at $2\rho_0$.

We do not present results obtained when assuming $M_{\rm max} = 1.3M_{\rm TOV}$ as these are essentially identical to the original constraints. To put that another way, GW190814's m_2 is barely consistent with a nonspinning NS, and therefore could impact our knowledge of the EOS, but it is perfectly consistent with a (possibly rapidly) spinning NS, in which case we cannot learn about the EOS without direct measurements of matter effects in the waveform.

All the results in this section come with the substantial caveat that we do not know that GW190814 was an NSBH coalescence, and therefore, we cannot assert that m_2 was an NS a priori without the possibility of substantially biasing our inference of the EOS. No EM counterpart was observed, although this in itself is inconclusive (Coughlin et al. 2019). Given the uncertainties in the shape of the overall mass distribution, the presence and depth of possible mass gaps, and even whether the lower edge of such mass gaps are related to $M_{\rm max}$, updated constraints on the EOS obtained by assuming m_2 was a nonspinning NS should be met with healthy skepticism. Indeed, the analyses in Section 4 suggest that m_2 is most consistent with either a spinning NS or a BH, and finer resolution is limited by the poor constraints on m_2's spin.

6. Discussion

In this paper, we investigated what knowledge of the total rate density of low-mass compact binary coalescences and uncertainty in the maximum NS mass, $M_{\rm max}$, can tell us about the nature of individual compact objects. While several matter signatures in the GW waveform can distinguish between types of low-mass stellar remnants, we expect that there will be a population of events for which these signatures are inconclusive and for which we will only be able to distinguish between types of objects based on their masses. Specifically, we showed that we can place an upper bound on the posterior probability that any object is an NS, but that different assumptions about the unknown prior odds between NSs and BHs below $M_{\rm max}$ could reduce our confidence that any particular object is an NS. As such, we can only definitively rule out, rather than establish, the presence of an NS in a given coalescence without further knowledge of the subpopulation mass distributions or direct observations of tidal signatures. Our hierarchical Bayesian approach generalizes previous mass-based classification schemes by not only including the full posterior distributions with population-informed priors but also accounting for our uncertainty in the mass that separates the NS and BH classes.

Applying this to two recent detections, we find that GW190425 was likely a BNS coalescence rather than an NSBH. Because of the signal's relatively low S/N and correspondingly broad uncertainty in the component masses, we find that different assumptions about the astrophysical distribution of masses in this range can affect our confidence more than the systematic uncertainty between different $M_{\rm max}$ distributions. Most populations we assume favor symmetric mass ratios and therefore smaller values for m_1. We typically find $P(m_1 \leqslant M_{\rm max})$ between 70% and 99%. Although we cannot definitely prove that GW190425 did not involve a BH and other plausible astrophysical scenarios have been proposed (Foley et al. 2020; Han et al. 2020), this is nonetheless suggestive.

Similarly, we find GW190814's m_2 was almost certainly not a nonspinning NS, as $P(m_2 \leqslant M_{\rm TOV}) \lesssim 6\%$ for $M_{\rm TOV}$ distributions based on NS EOS studies. While we find that m_2 is completely consistent with an NS spinning near its breakup frequency, we also note that the data does not constrain m_2's spin. This agrees with the analysis presented in Abbott et al. (2020b). Any higher-dimensional inference will be dominated by assumptions about the spin distribution. For example, Most et al. (2020) place lower bounds on $M_{\rm TOV}$ and the secondary's spin under the assumption that the object must lie near the universal relation for $M_{\rm max}(M_{\rm TOV}, \chi)$ (Breu & Rezzolla 2016), motivated by the belief that it could not have accreted much mass after it was initially formed.

These GW events emphasize the different limiting outcomes that can be expected in such an inference, when the knowledge of component masses is either significantly larger or smaller than the uncertainty in $M_{\rm max}$. Unsurprisingly, the systematic uncertainty associated with whichever distribution is larger dominates the uncertainty in our conclusions. As such, even perfect knowledge of the component masses for a particular event will not remove all systematic uncertainties, as several estimates for $M_{\rm max}$ exist. At the same time, perfect knowledge of $M_{\rm max}$ simply means we will be limited by our understanding of how the population of low-mass stellar remnants is distributed. This uncertainty could have a significant impact on our conclusions and should not be ignored.

Although universal relations connect the maximum mass of nonspinning NSs, $M_{\rm TOV}$, and how much more mass can be supported by the object's spin, it is not known how reliable these relations are in the presence of strong phase transitions. Improving our theoretical understanding of this separatrix is unlikely to improve our understanding of GW190425 but could be useful for GW190814. Specifically, using the universal relation for $M_{\rm max}(M_{\rm TOV}, \chi)$ from Breu & Rezzolla (2016), we argue that a mass that is almost surely above $M_{\rm TOV}$ may suggest the object could not have been an NS, as $M_{\rm max}$ may only significantly exceed $M_{\rm TOV}$ when the spins reach implausibly large amplitudes. Most et al. (2020) arrive at a similar conclusion; assuming m_2 was an NS, they find it may have been the fastest spinning NS ever observed.

We also present a few caveats to keep in mind for this type of analysis. Foremost is the fact that, although it may intuitively

seem sensible to base classification on a Bayes factor to minimize the possible impact of prior beliefs, we show that Bayes factors are sensitive to the high-mass behavior of the BH mass distribution, which should be irrelevant for low-mass objects. Using the posterior odds, or odds ratios, avoids this shortcoming as it only depends on the prior within the likelihood's support. Furthermore, real binaries may come from a variety of formation channels, each of which may produce different distributions for BNSs, BBHs, and NSBH systems. These formation channels may limit the maximum mass attained by astrophysical NSs to $m \leqslant M_{\rm form} \leqslant M_{\rm max}$. We argue that we are likely to only measure the sum of these distributions directly from the data and make the simplifying assumption that $M_{\rm form} = M_{\rm max}$. More detailed knowledge of individual subpopulations would likely be extremely useful. Mandel et al. (2015, 2016) investigate such knowledge from a single population synthesis calculation, finding that precise knowledge of subpopulations could obviate the classification problem, allowing most systems to be identified "by eye" or with simple clustering algorithms from the masses alone without the need for the formal machinery developed here.

Looking forward, Fishbach et al. (2020a) suggest that we should expect as many as one out of every six detections to involve a primary mass $\lesssim 7\,M_\odot$ and that a significant fraction of these may have ambiguous classifications based on their masses alone. Indeed, existing public alerts from O3 (The LIGO Scientific Collaboration & The Virgo Collaboration 2020b) include several candidates classified as likely to contain possibly ambiguous components (BNS, NSBH, and Mass Gap events as defined in The LIGO Scientific Collaboration & The Virgo Collaboration 2020a). We therefore expect the statistical and systematic uncertainties explored here to remain relevant throughout the advanced detector era, although Chen et al. (2020) show that we should expect to relatively confidently detect tidal signatures for nearby systems with the expected O4 detector sensitivities.

Indeed, although the S/N distribution of compact binary systems observed with third-generation detectors will peak above the detection threshold (see Figure 7 of Vitale 2016) and a much larger fraction of detections will have clearly discernible matter signatures within their waveforms, a nontrivial fraction will still have low-enough S/N that their masses may be our best way to identify their constituents.

Nonetheless, even bearing in mind the systematic uncertainties from our imperfect knowledge of the distribution of low-mass stellar remnants and the EOS of dense nuclear matter, it is remarkable that GW observations already allow us to ask such pointed questions about individual astrophysical objects so soon after the first direct detection of GWs (Abbott et al. 2016). This demonstrates the vast amount of information encoded within GW signals and the unprecedented opportunities they provide to learn about astrophysical population of compact objects.

The authors thank Jolien Creighton, Maya Fishbach, and Daniel Holz for their feedback while preparing this manuscript. The authors are also grateful for useful discussions with Katerina Chatziioannou and the broader LIGO-Virgo-KAGRA Extreme Matter and Rates & Populations working groups. R.E. is supported at the University of Chicago by the Kavli Institute for Cosmological Physics through an endowment from the Kavli Foundation and its founder Fred Kavli. P.L. is supported by National Science Foundation award PHY-1836734 and by a gift from the Black Family Trust to the Gravitational-Wave Physics & Astronomy Center. The authors also gratefully acknowledge the computational resources provided by the LIGO Laboratory and supported by NSF grants PHY-0757058 and PHY-0823459.

Appendix
Monte Carlo Integrals

Some of our Monte Carlo integral expressions are nontrivial, and as such, we report them below. We begin with the assumption that we have weighted sets of samples for $M_{\rm max}$ and the mass of an individual object. For example, given $x_i \sim p(x)$, we expect

$$\frac{1}{N}\sum_i^N \mathcal{F}(x_i) \approx \int dx\, p(x)\mathcal{F}(x) \tag{A1}$$

with $\mathcal{F}(x)$ an arbitrary function of x. The basic quantity of interest in our calculation is

$$P(m \leqslant M) = \frac{f}{g}, \tag{A2}$$

where

$$f = \frac{1}{N_M}\sum_i^{N_M} p(\mathcal{D}_{\rm EOS}|M_i)\frac{1}{N_m}\sum_k^{N_m}\frac{p(m_k|\mathcal{H})}{p(m_k|\mathcal{H}_o)}{\rm H}(m_k \leqslant M_i) \tag{A3}$$

$$g = \frac{1}{N_M}\sum_i^{N_M} p(\mathcal{D}_{\rm EOS}|M_i)\frac{1}{N_m}\sum_k^{N_m}\frac{p(m_k|\mathcal{H})}{p(m_k|\mathcal{H}_o)} \tag{A4}$$

assuming $M_i \sim p(M)$ and $m_k \sim p(m|\mathcal{D}, \mathcal{H}_o)$ so that the integrals are done with respect to the measures $p(M|\mathcal{D}_{\rm EOS}) \propto p(M)p(\mathcal{D}_{\rm EOS}|M)$ and $p(m|\mathcal{D}, \mathcal{H}) \propto p(m|\mathcal{D}, \mathcal{H}_o)p(m|\mathcal{H})/p(m|\mathcal{H}_o)$, respectively. This approximates the types of Monte Carlo integrals over the EOS realizations drawn from a prior done in Landry et al. (2020) as well as the process of reweighing single-event posteriors generated with one prior $\mathcal{H}_o$ to match a different population prior $\mathcal{H}$. We investigate the behavior of these estimators and their correlated uncertainty from the finite number of Monte Carlo samples.

Let us begin with g. Its first and second moments under different realizations of sample sets are given by

$$\begin{aligned}\mathcal{E}[g] &= \int \prod_i dM_i\, p(M_i) \prod_k dm_k\, p(m_k|\mathcal{D}, \mathcal{H}_o) \\ &\quad\times \frac{1}{N_M}\sum_j^{N_M} p(\mathcal{D}_{\rm EOS}|M_j)\frac{1}{N_m}\sum_l^{N_m}\frac{p(m_l|\mathcal{D}, \mathcal{H})}{p(m_l|\mathcal{D}, \mathcal{H}_o)} \\ &= \left(\int dM\, p(M)p(\mathcal{D}_{\rm EOS}|M)\right) \\ &\quad\times \left(\int dm\, p(m|\mathcal{D}, \mathcal{H}_o)\frac{p(m|\mathcal{H})}{p(m|\mathcal{H}_o)}\right) \\ &= p(\mathcal{D}_{\rm EOS})\left(\frac{p(\mathcal{D}|\mathcal{H})}{p(\mathcal{D}|\mathcal{H}_o)}\right),\end{aligned} \tag{A5}$$

$$\begin{aligned}\mathcal{E}[g^2] &= \int \prod_i dM_i\, p(M_i) \prod_k dm_k\, p(m_k|\mathcal{D}, \mathcal{H}_o) \\ &\quad \times \left[\frac{1}{N_M}\sum_j^{N_M} p(\mathcal{D}_{\rm EOS}|M_j)\frac{1}{N_m}\sum_l^{N_m}\frac{p(m_l|\mathcal{H})}{p(m_l|\mathcal{H}_o)}\right]^2 \\ &= \frac{1}{N_M N_m}\left(\int dM\; p(M)p(\mathcal{D}_{\rm EOS}|M)^2\right) \\ &\quad \times \left(\int dm\; p(m|\mathcal{D}, \mathcal{H}_o)\left(\frac{p(m|\mathcal{H})}{p(m|\mathcal{H}_o)}\right)^2\right) \\ &\quad + \frac{N_m - 1}{N_M N_m}\left(\int dM\; p(M)p(\mathcal{D}_{\rm EOS}|M)^2\right) \\ &\quad \times \left(\int dm\; p(m|\mathcal{D}, \mathcal{H}_o)\frac{p(m|\mathcal{H})}{p(m|\mathcal{H}_o)}\right)^2 \\ &\quad + \frac{N_M - 1}{N_M N_m}\left(\int dM\; p(M)p(\mathcal{D}_{\rm EOS}|M)\right)^2 \\ &\quad \times \left(\int dm\; p(m|\mathcal{D}, \mathcal{H}_o)\left(\frac{p(m|\mathcal{H})}{p(m|\mathcal{H}_o)}\right)^2\right) \\ &\quad + \frac{(N_M - 1)(N_m - 1)}{N_M N_m}\left(\int dM\; p(M)p(\mathcal{D}_{\rm EOS}|M)\right)^2 \\ &\quad \times \left(\int dm\; p(m|\mathcal{D}, \mathcal{H}_o)\frac{p(m|\mathcal{H})}{p(m|\mathcal{H}_o)}\right)^2. \end{aligned} \tag{A6}$$

Similarly, we obtain

$$\begin{aligned}\mathcal{E}[f] &= \int dMdm\; p(M)p(\mathcal{D}_{\rm EOS}|M)p(m|\mathcal{D}, \mathcal{H}_o) \\ &\quad \times \frac{p(m|\mathcal{H})}{p(m|\mathcal{H}_o)}\mathrm{H}(m \leqslant M)\end{aligned} \tag{A7}$$

$$\begin{aligned}\mathcal{E}[f^2] &= \frac{1}{N_M N_m}\int dMdm\; p(M)p(\mathcal{D}_{\rm EOS}|M)^2 p(m|\mathcal{D}, \mathcal{H}_o) \\ &\quad \times \left(\frac{p(m|\mathcal{H})}{p(m|\mathcal{H}_o)}\right)^2 \mathrm{H}(m \leqslant M) \\ &\quad + \frac{N_m - 1}{N_M N_m}\int dM\; p(M)p(\mathcal{D}_{\rm EOS}|M)^2 \\ &\quad \times \left(\int dm\; p(m|\mathcal{D}, \mathcal{H}_o)\frac{p(m|\mathcal{H})}{p(m|\mathcal{H}_o)}\mathrm{H}(m \leqslant M)\right)^2 \\ &\quad + \frac{N_M - 1}{N_M N_m}\int dm\; p(m|\mathcal{D}, \mathcal{H}_o)\left(\frac{p(m|\mathcal{H})}{p(m|\mathcal{H}_o)}\right)^2 \\ &\quad \times \left(\int dM\; p(M)p(\mathcal{D}_{\rm EOS}|M)\mathrm{H}(m \leqslant M)\right)^2 \\ &\quad + \frac{(N_M - 1)(N_m - 1)}{N_M N_m} \\ &\quad \times \left(\int dMdm\; p(M)p(\mathcal{D}_{\rm EOS}|M)p(m|\mathcal{D}, \mathcal{H}_o)\right. \\ &\quad \left. \times \frac{p(m|\mathcal{H})}{p(m|\mathcal{H}_o)}\mathrm{H}(m \leqslant M)\right)^2, \end{aligned} \tag{A8}$$

$$\begin{aligned}\mathcal{E}[fg] &= \frac{1}{N_M N_m}\int dMdm\; p(M)p(\mathcal{D}_{\rm EOS}|M)^2 p(m|\mathcal{D}, \mathcal{H}_o) \\ &\quad \times \left(\frac{p(m|\mathcal{H})}{p(m|\mathcal{H}_o)}\right)^2 \mathrm{H}(m \leqslant M) \\ &\quad + \frac{N_m - 1}{N_M N_m}\int dM\; p(M)p(\mathcal{D}_{\rm EOS}|M)^2 \\ &\quad \times \left(\int dm\; p(m|\mathcal{D}, \mathcal{H}_o)\frac{p(m|\mathcal{H})}{p(m|\mathcal{H}_o)}\mathrm{H}(m \leqslant M)\right) \\ &\quad \times \left(\int dm\; p(m|\mathcal{D}, \mathcal{H}_o)\frac{p(m|\mathcal{H})}{p(m|\mathcal{H}_o)}\right) \\ &\quad + \frac{N_M - 1}{N_M N_m}\int dm\; p(m|\mathcal{D}, \mathcal{H}_o)\left(\frac{p(m|\mathcal{H})}{p(m|\mathcal{H}_o)}\right)^2 \\ &\quad \times \left(\int dM\; p(M)p(\mathcal{D}_{\rm EOS}|M)\mathrm{H}(m \leqslant M)\right) \\ &\quad \times \left(\int dM\; p(M)p(\mathcal{D}_{\rm EOS}|M)\right) \\ &\quad + \frac{(N_M - 1)(N_m - 1)}{N_M N_m} \\ &\quad \times \left(\int dMdm\; p(M)p(\mathcal{D}_{\rm EOS}|M)p(m|\mathcal{D}, \mathcal{H}_o)\right. \\ &\quad \left. \times \frac{p(m|\mathcal{H})}{p(m|\mathcal{H}_o)}\mathrm{H}(m \leqslant M)\right) \\ &\quad \times \left(\int dMdm\; p(M)p(\mathcal{D}_{\rm EOS})p(m|\mathcal{D}, \mathcal{H}_o)\frac{p(m|\mathcal{H})}{p(m|\mathcal{H}_o)}\right). \end{aligned} \tag{A9}$$

These expressions are exact, but as we may not be able to analytically integrate $p(M)p(\mathcal{D}_{\rm EOS}|M)$ or $p(m|\mathcal{D}, \mathcal{H})$, we approximate each with Monte Carlo sums. This implies the first moments are approximated by Equations (A16) and (A17), while the second moments are approximately

$$\begin{aligned}\mathcal{E}[f^2] &\approx \frac{1}{N_M^2 N_m^2}\sum_i^{N_M}\sum_k^{N_m} p(\mathcal{D}_{\rm EOS}|M_i)^2\left(\frac{p(m_k|\mathcal{H})}{p(m_k|\mathcal{H}_o)}\right)^2 \mathrm{H}(m_k \leqslant M_i) \\ &\quad + \frac{N_m - 1}{N_M^2 N_m^3}\sum_i^{N_M} p(\mathcal{D}_{\rm EOS}|M_i)^2\left(\sum_k^{N_m}\frac{p(m_k|\mathcal{H})}{p(m_k|\mathcal{H}_o)}\mathrm{H}(m_k \leqslant M_i)\right)^2 \\ &\quad + \frac{N_M - 1}{N_M^3 N_m^2}\sum_k^{N_m}\left(\frac{p(m_k|\mathcal{H})}{p(m_k|\mathcal{H}_o)}\right)^2\left(\sum_i^{N_M} p(\mathcal{D}_{\rm EOS}|M_i)\mathrm{H}(m_k \leqslant M_i)\right)^2 \\ &\quad + \frac{(N_M - 1)(N_m - 1)}{N_M^3 N_m^3}\left(\sum_i^{N_M}\sum_k^{N_m} p(\mathcal{D}_{\rm EOS}|M_i)\frac{p(m_k|\mathcal{H})}{p(m_k|\mathcal{H}_o)}\mathrm{H}(m_k \leqslant M_i)\right)^2 \end{aligned} \tag{A10}$$

$$\begin{aligned}\mathcal{E}[g^2] &\approx \frac{1}{N_M^2 N_m^2}\left(\sum_i^{N_M} p(\mathcal{D}_{\rm EOS}|M_i)^2\right)\left(\sum_k^{N_m}\left(\frac{p(m_k|\mathcal{H})}{p(m_k|\mathcal{H}_o)}\right)^2\right) \\ &\quad + \frac{N_m - 1}{N_M^2 N_m^3}\left(\sum_i^{N_M} p(\mathcal{D}_{\rm EOS}|M_i)^2\right)\left(\sum_k^{N_m}\frac{p(m_k|\mathcal{H})}{p(m_k|\mathcal{H}_o)}\right)^2 \\ &\quad + \frac{N_M - 1}{N_M^3 N_m^2}\left(\sum_i^{N_M} p(\mathcal{D}_{\rm EOS}|M_i)\right)^2\left(\sum_k^{N_m}\left(\frac{p(m_k|\mathcal{H})}{p(m_k|\mathcal{H}_o)}\right)^2\right) \\ &\quad + \frac{(N_M - 1)(N_m - 1)}{N_M^3 N_m^3}\left(\sum_i^{N_M} p(\mathcal{D}_{\rm EOS}|M_i)\right)^2\left(\sum_k^{N_m}\frac{p(m_k|\mathcal{H})}{p(m_k|\mathcal{H}_o)}\right)^2 \end{aligned} \tag{A11}$$

$$
\begin{aligned}
\mathcal{E}[fg] \approx & \frac{1}{N_M^2 N_m^2}\sum_i^{N_M}\sum_k^{N_m} p(\mathcal{D}_{\rm EOS}|M_i)^2\left(\frac{p(m_k|\mathcal{H})}{p(m_k|\mathcal{H}_o)}\right)^2 \\
& \times \mathcal{H}(m_k \leqslant M_i) \\
& + \frac{N_m - 1}{N_M^2 N_m^3}\sum_i^{N_M} p(\mathcal{D}_{\rm EOS}|M_i)^2\left(\sum_k^{N_m}\frac{p(m_k|\mathcal{H})}{p(m_k|\mathcal{H}_o)}{\rm H}(m_k \leqslant M_i)\right) \\
& \times \left(\sum_l^{N_m}\frac{p(m_l|\mathcal{H})}{p(m_l|\mathcal{H}_o)}\right) \\
& + \frac{N_M - 1}{N_M^3 N_m^2}\sum_k^{N_m}\left(\frac{p(m_k|\mathcal{H})}{p(m_k|\mathcal{H}_o)}\right)^2\left(\sum_i^{N_M} p(\mathcal{D}_{\rm EOS}|M_i){\rm H}(m_k \leqslant M_i)\right) \\
& \times \left(\sum_j^{N_M} p(\mathcal{D}_{\rm EOS}|M_j)\right) \\
& + \frac{(N_M - 1)(N_m - 1)}{N_M^3 N_m^3}\left(\sum_i^{N_M}\sum_k^{N_m} p(\mathcal{D}_{\rm EOS}|M_i)\right. \\
& \left. \times \frac{p(m_k|\mathcal{H})}{p(m_k|\mathcal{H}_o)}{\rm H}(m_k \leqslant M_i)\right) \\
& \times \left(\sum_i^{N_M} p(\mathcal{D}_{\rm EOS}|M_i)\right)\left(\sum_k^{N_m}\frac{p(m_k|\mathcal{H})}{p(m_k|\mathcal{H}_o)}\right).
\end{aligned}
\tag{A12}
$$

Equipped with these uncertainty estimates, we approximate our statistics as follows

$$
P(m \leqslant M) = \frac{\mathcal{E}[f]}{\mathcal{E}[g]} \pm \sqrt{(\mathcal{E}[f^2] - \mathcal{E}[f]^2)\frac{1}{\mathcal{E}[g]^2} + (\mathcal{E}[g^2] - \mathcal{E}[g]^2)\frac{\mathcal{E}[f]^2}{\mathcal{E}[g]^4} - 2(\mathcal{E}[fg] - \mathcal{E}[f]\mathcal{E}[g])\frac{\mathcal{E}[f]}{\mathcal{E}[g]^3}}
\tag{A13}
$$

$$
\begin{aligned}
\mathcal{O}_{m>M}^{m\leqslant M} &= \frac{P(m \leqslant M)}{1 - P(m \leqslant M)} = \frac{\mathcal{E}[f]}{\mathcal{E}[g] - \mathcal{E}[f]} \\
&\pm \sqrt{(\mathcal{E}[f^2] - \mathcal{E}[f]^2)\frac{\mathcal{E}[g]^2}{(\mathcal{E}[g] - \mathcal{E}[f])^4} + (\mathcal{E}[g^2] - \mathcal{E}[g]^2)\frac{\mathcal{E}[f]^2}{(\mathcal{E}[g] - \mathcal{E}[f])^4} - 2(\mathcal{E}[fg] - \mathcal{E}[f]\mathcal{E}[g])\frac{\mathcal{E}[g]\mathcal{E}[f]}{(\mathcal{E}[g] - \mathcal{E}[f])^4}}.
\end{aligned}
\tag{A14}
$$

We note that similar error estimates are possible for $\mathcal{B}_{m>M}^{m\leqslant M}$ via Monte Carlo approximates to

$$
\mathcal{B}_{m>M}^{m\leqslant M} = \left(\frac{f}{g - f}\right)\left(\frac{\mathcal{G} - \mathcal{F}}{\mathcal{F}}\right),
\tag{A15}
$$

where

$$
\mathcal{F} = \frac{1}{N_M}\sum_i^{N_M} p(\mathcal{D}_{\rm EOS}|M_i)\frac{1}{N_p}\sum_j^{N_p}\frac{p(m_j|\mathcal{H})}{p(m_j|\mathcal{H}_o)}{\rm H}(m_j \leqslant M_i),
\tag{A16}
$$

$$
\mathcal{G} = \frac{1}{N_M}\sum_i^{N_M} p(\mathcal{D}_{\rm EOS}|M_i)\frac{1}{N_p}\sum_j^{N_p}\frac{p(m_j|\mathcal{H})}{p(m_j|\mathcal{H}_o)},
\tag{A17}
$$

where the N_p mass samples are drawn from the single-event prior ($m_k \sim p(m|\mathcal{H}_o)$) instead of the posterior. This follows from separate estimates from the posterior odds and prior odds in Equations (10) and (14). We use a similar decomposition into separate (correlated) Monte Carlo estimates for the numerator and denominator of the posterior and prior odds separately as well as cross-terms from the fact that we use the same set of $M_{\rm max}$ samples within both estimates. However, as we do not report $\mathcal{B}_{m>M}^{m\leqslant M}$ within our analysis, we leave the technical details as an exercise for the reader.

ORCID iDs

Reed Essick https://orcid.org/0000-0001-8196-9267
Philippe Landry https://orcid.org/0000-0002-8457-1964

References

Aasi, J., Abbott, B. P., Abbott, R., et al. 2015, CQGra, 32, 074001
Abbott, B. P., Abbott, R., Abbott, T. D., et al. 2019, PhRvX, 9, 011001
Abbott, B. P., Abbott, R., Abbott, T. D., et al. 2020, ApJL, 892, L3
Abbott, B. P., Abbott, R., Abbott, T. D., et al. 2016, PhRvL, 116, 061102
Abbott, B. P., Abbott, R., Abbott, T. D., et al. 2017a, PhRvL, 119, 161101
Abbott, B. P., Abbott, R., Abbott, T. D., et al. 2017b, ApJL, 848, L12
Abbott, B. P., Abbott, R., Abbott, T. D., et al. 2017c, ApJL, 850, L39
Abbott, B. P., Abbott, R., Abbott, T. D., et al. 2018, PhRvL, 121, 161101
Abbott, B. P., Abbott, R., Abbott, T. D., et al. 2019a, PhRvL, 122, 061104
Abbott, B. P., Abbott, R., Abbott, T. D., et al. 2019b, PhRvX, 9, 031040
Abbott, B. P., Abbott, R., Abbott, T. D., et al. 2019c, ApJL, 882, L24
Abbott, B. P., Abbott, R., Abbott, T. D., et al. 2020a, CQGra, 37, 045006
Abbott, R., Abbott, T. D., Abraham, S., et al. 2020b, ApJL, 896, L44
Acernese, F., Acernese, F., Agathos, M., Agatsuma, K., et al. 2015, CQGra, 32, 024001
Ai, S., Gao, H., & Zhang, B. 2020, ApJ, 893, 146
Alsing, J., Silva, H. O., & Berti, E. 2018, MNRAS, 478, 1377
Antoniadis, J., Freire, P. C., Wex, N., et al. 2013, Sci, 340, 1233232
Antoniadis, J., Tauris, T. M., Ozel, F., et al. 2016, arXiv:1605.01665
Bailyn, C. D., Jain, R. K., Coppi, P., & Orosz, J. A. 1998, ApJ, 499, 367
Barbieri, C., Salafia, O. S., Colpi, M., Ghirlanda, G., & Perego, A. 2020, arXiv:2002.09395
Barbieri, C., Salafia, O. S., Perego, A., Colpi, M., & Ghirlanda, G. 2019, A&A, 625, A152
Bauswein, A., Baumgarte, T. W., & Janka, H.-T. 2013, PhRvL, 111, 131101
Belczynski, K., Wiktorowicz, G., Fryer, C. L., Holz, D. E., & Kalogera, V. 2012, ApJ, 757, 91
Breu, C., & Rezzolla, L. 2016, MNRAS, 459, 646
Bulik, T., Belczynski, K., & Kalogera, V. 2003, Proc. SPIE, 4856, 146
Cardoso, V., & Pani, P. 2019, LRR, 22, 4
Carney, M. F., Wade, L. E., & Irwin, B. S. 2018, PhRvD, 98, 063004
Carr, B. J., & Hawking, S. W. 1974, MNRAS, 168, 399
Chatziioannou, K., & Farr, W. M. 2020, PhRvD, 102, 064063
Chen, A., Johnson-McDaniel, N. K., Dietrich, T., & Dudi, R. 2020, PhRvD, 101, 103008
Chen, H.-Y., & Chatziioannou, K. 2020, ApJL, 893, L41
Cook, G. B., Shapiro, S. L., & Teukolsky, S. A. 1994, ApJ, 424, 823
Coughlin, M. W., & Dietrich, T. 2019, PhRvD, 100, 043011
Coughlin, M. W., Dietrich, T., Antier, S., et al. 2019, MNRAS, 492, 863
Cromartie, H. T., Fonseca, E., Ransom, S. M., et al. 2020, NatAs, 4, 72
Datta, S., Phukon, K. S., & Bose, S. 2020, arXiv:2004.05974
Dietrich, T., Coughlin, M. W., Pang, P. T. H., et al. 2020, arXiv:2002.11355
Ertl, T., Woosley, S. E., Sukhbold, T., & Janka, H.-T. 2020, ApJ, 890, 51
Essick, R., Landry, P., & Holz, D. E. 2020, PhRvD, 101, 063007
Essick, R., Vitale, S., & Weinberg, N. N. 2016, PhRvD, 94, 103012
Farr, W. M., & Chatziioannou, K. 2020, RNAAS, 4, 65
Farr, W. M., Gair, J. R., Mandel, I., & Cutler, C. 2015, PhRvD, 91, 023005
Farr, W. M., Sravan, N., Cantrell, A., et al. 2011, ApJ, 741, 103
Farrow, N., Zhu, X.-J., & Thrane, E. 2019, ApJ, 876, 18
Fasano, M., Wong, K. W. K., Maselli, A., et al. 2020, PhRvD, 102, 023025
Fernández, R., Foucart, F., Kasen, D., et al. 2017, CQGra, 34, 154001
Fishbach, M., Essick, R., & Holz, D. E. 2020a, ApJ, 899, 8
Fishbach, M., Farr, W. M., & Holz, D. E. 2020b, ApJL, 891, L31
Fishbach, M., & Holz, D. E. 2017, ApJL, 851, L25
Fishbach, M., & Holz, D. E. 2020, ApJL, 891, L27
Flanagan, E. E., & Hinderer, T. 2008, PhRvD, 77, 021502
Foley, R. J., Coulter, D. A., Kilpatrick, C. D., et al. 2020, MNRAS, 494, 190
Foucart, F., Hinderer, T., & Nissanke, S. 2018, PhRvD, 98, 081501
Fryer, C. L., & Kalogera, V. 2001, ApJ, 554, 548
Gopalan, G., Vrtilek, S. D., & Bornn, L. 2015, ApJ, 809, 40
Gupta, A., Gerosa, D., Arun, K. G., et al. 2020, PhRvD, 101, 103036
Haensel, P., Salgado, M., & Bonazzola, S. 1995, A&A, 296, 745
Han, M.-Z., Tang, S.-P., Hu, Y.-M., et al. 2020, ApJL, 891, L5
Hannam, M., Brown, D. A., Fairhurst, S., Fryer, C. L., & Harry, I. W. 2013, ApJL, 766, L14
Haster, C.-J., Chatziioannou, K., Bauswein, A., & Clark, J. A. 2020, arXiv:2004.11334
Hessels, J. W. T., Ransom, S. M., Stairs, I. H., et al. 2006, Sci, 311, 1901
Hinderer, T., Nissanke, S., Foucart, F., et al. 2019, PhRvD, 100, 063021
Hinderer, T., Taracchini, A., Foucart, F., et al. 2016, PhRvL, 116, 181101
Johnson-McDaniel, N. K., Mukherjee, A., Kashyap, R., et al. 2018, arXiv:1804.08026
Kapadia, S. J., Caudill, S., Creighton, J. D. E., et al. 2020, CQGra, 37, 045007
Krishnendu, N. V., Arun, K. G., & Mishra, C. K. 2017, PhRvL, 119, 091101
Krishnendu, N. V., Saleem, M., Samajdar, A., et al. 2019, PhRvD, 100, 104019
Kyutoku, K., Fujibayashi, S., Hayashi, K., et al. 2020, ApJL, 890, L4
Lackey, B. D., & Wade, L. 2015, PhRvD, 91, 043002
Lai, D. 1994, MNRAS, 270, 611
Landry, P., Essick, R., & Chatziioannou, K. 2020, PhRvD, 101, 123007
Lattimer, J. M., & Prakash, M. 2001, ApJ, 550, 426
Littenberg, T. B., Farr, B., Coughlin, S., Kalogera, V., & Holz, D. E. 2015, ApJL, 807, L24
Loredo, T. J. 2004, in AIP Conf. Ser. 735, Bayesian Inference and Maximum Entropy Methods in Science and Engineering, ed. R. Fischer, R. Preuss, & U. V. Toussaint (Melville, NY: AIP), 195
Loredo, T. J., & Wasserman, I. M. 1995, ApJS, 96, 261
Mandel, I., & Farmer, A. 2018, arXiv:1806.05820
Mandel, I., Farr, W. M., Colonna, A., et al. 2016, MNRAS, 465, 3254
Mandel, I., Farr, W. M., & Gair, J. R. 2019, MNRAS, 486, 1086
Mandel, I., Haster, C.-J., Dominik, M., & Belczynski, K. 2015, MNRAS, 450, L85
Margalit, B., & Metzger, B. D. 2017, ApJL, 850, L19
Margalit, B., & Metzger, B. D. 2019, ApJL, 880, L15
Meszaros, P. 1974, A&A, 37, 225
Miller, M. C., Chirenti, C., & Lamb, F. K. 2019a, ApJ, 888, 12
Miller, M. C., Lamb, F. K., Dittmann, A. J., et al. 2019b, ApJL, 887, L24
Most, E. R., Papenfort, L. J., Weih, L. R., & Rezzolla, L. 2020, MNRAS, 499, L82
Özel, F., Psaltis, D., Narayan, R., & McClintock, J. E. 2010, ApJ, 725, 1918
Postnov, K. A., & Yungelson, L. R. 2014, LRR, 14, 1433
Raaijmakers, G., Riley, T. E., Watts, A. L., et al. 2019, ApJL, 887, L22
Read, J. S., Lackey, B. D., Owen, B. J., & Friedman, J. L. 2009, PhRvD, 79, 124032
Reisenegger, A., & Goldreich, P. 1994, ApJ, 426, 688
Rezzolla, L., Most, E. R., & Weih, L. R. 2018, ApJL, 852, L25
Rhoades, C. E., & Ruffini, R. 1974, PhRvL, 32, 324
Riley, T. E., Watts, A. L., Bogdanov, S., et al. 2019, ApJL, 887, L21
Rodriguez, C. L., Amaro-Seoane, P., Chatterjee, S., et al. 2018, PhRvD, 98, 123005
Rodriguez, C. L., Zevin, M., Amaro-Seoane, P., et al. 2019, PhRvD, 100, 043027
Shibata, M., & Taniguchi, K. 2008, PhRvD, 77, 084015
Shibata, M., Zhou, E., Kiuchi, K., & Fujibayashi, S. 2019, PhRvD, 100, 023015
Steinhoff, J., Hinderer, T., Buonanno, A., & Taracchini, A. 2016, PhRvD, 94, 104028
Tan, H., Noronha-Hostler, J., & Yunes, N. 2020, arXiv:2006.16296
The LIGO Scientific Collaboration, & The Virgo Collaboration 2020a, LIGO/Virgo Public Alerts User Guide, https://emfollow.docs.ligo.org/userguide/
The LIGO Scientific Collaboration, & The Virgo Collaboration 2020b, Gravitational Wave Candidate Event DataBase, https://gracedb.ligo.org/
The LIGO Scientific Collaboration, & The Virgo Collaboration 2020c, Parameter Estimation Sample Release for GW190425, https://dcc.ligo.org/LIGO-P2000026/public
The LIGO Scientific Collaboration, & The Virgo Collaboration 2020d, GW190814 Parameter Estimation Samples, https://dcc.ligo.org/LIGO-P2000183/public
Tsokaros, A., Ruiz, M., Shapiro, S. L., Sun, L., & Uryū, K. 2020, PhRvL, 124, 071101
Van Oeveren, E. D., & Friedman, J. L. 2017, PhRvD, 95, 083014
Vitale, S. 2016, PhRvD, 94, 121501
Weinberg, N. N. 2016, ApJ, 819, 109
Wysocki, D., O'Shaughnessy, R., Wade, L., & Lange, J. 2020, arXiv:2001.01747
Yang, H., East, W. E., & Lehner, L. 2018, ApJ, 856, 110